AAAS

Science

15 MAY 2025

ON THE MOVE

Connectivity of Pleistocene horse populations across Beringia and beyond p. 748

PALEONTOLOGY

Sustainability insights from Late Pleistocene climate change and horse migration patterns

Yvette Running Horse Collin (Tašunke Iyanke Wiŋ)[1,2,3]*, Clément P. Bataille[4,5]*, Samantha Hershauer[6], Mila Hunska Tašunke Icu (Chief Joe American Horse)[2,3], (Akil Nujipi) Chief Harold Left Heron[2,3], Wilson Justin[7,8,9], Jane (q^{w}yxnmitk^{w}) Stelkia[10], C'wyelx (Thomas Pierre)[11], James Aaron Stelkia[12], Sean Asikłuk Topkok[13], Beth Ginondidoy Leonard[14,15], Beatle (Naatoonistaahs) Soop[16], Mario Gonzalez (Nantan Hinapan)[2,3], Anpetu Luta Wiŋ (Antonia Loretta Afraid of Bear-Cook)[2,3], Wakiŋyala Wiŋ (Anita Afraid of Bear)[2,3], Tanka Omniya (Robert Milo Yellow Hair)[2,3], Barbara Dull Knife (Mah'piya Keyaké Wiŋ)[2,3], Mažasu (Wendell W. Yellow Bull)[2,3], Bill Means[2,3], Cruz Tecumseh Collin (Wanka'tuya Kiya)[2,3], Michael Koskey[12], Joshua D. Kapp[17], Zoe Landry[4], Danielle Fraser[18,19,20], John Southon[21], Eve E. Lindroos[4], Auguste Hassler[4,22], Lorelei Chauvey[1], Gaetan Tressières[1], Laure Tonasso-Calvière[1], Stéphanie Schiavinato[1], Andaine Seguin-Orlando[1], Aude Perdereau[23], Pedro H. Oliveira[24], Jean-Marc Aury[24], Patrick Wincker[24], Irina V. Kirillova[25], Sergey K. Vasiliev[26], Mariya A. Kusliy[1,27], Alexander S. Graphodatsky[27], Alexey A. Tishkin[28], Ian Barnes[29], Pat Druckenmiller[30,31], Christopher N. Jass[32], Ross D. E. MacPhee[33], Christina I. Barrón-Ortiz[32], Pam Groves[34], Dan Mann[33], Duane G. Froese[35], Matthew Wooller[36], Joshua H. Miller[20,37], Brooke Crowley[37,38], Grant Zazula[39], Elizabeth Hall[39], Susan Hewitson[39], Beth Shapiro[17]*, Ludovic Orlando[1]*

Climate affects habitat, food availability, and the movement and sustainability of all life. In this work, we apply Indigenous and Western scientific methods, including genomics and isotope profiling, on fossils from across Beringia to explore the effect of climate change on horses. We find that Late Pleistocene horses from Alaska and northern Yukon are related to populations from Eurasia and crossed the Bering land bridge multiple times during the last glacial interval. We also find deeply divergent lineages north and south of the American ice sheets that genetically influenced populations across Beringia and into Eurasia. As climate warmed and horses entered the ice-free corridor connecting Beringia and midcontinental America, restricted mobility and food availability impeded population growth. Our combined Western and Indigenous framework offers critical guidance for wildlife conservation amid ongoing climate change.

Many Indigenous scientific systems are premised on the knowledge that all life is in constant motion (*1*), moving and adapting as climate shifts (*2*). Megafauna (animals that are >45 kg) fill keystone roles in ecosystems, shaping biodiversity (*3*) and safeguarding carbon stocks in soils and vegetation (*4*). Their decline can trigger cascading effects on ecosystem function, habitats, and people (*5*, *6*). This is especially acute in the Arctic, which is warming considerably faster compared with other ecosystems (*7*, *8*). Understanding the long-term interplay between megafaunal dynamics and climate change is urgently needed to aid conservation and ecosystem restoration in the Artic and beyond (*9*).

Indigenous science has accumulated invaluable knowledge on habitat change and its effects on the movement of peoples, megafauna, and other life forms (*10*, *11*). The fossil record—with its deep temporal archive of responses to changing environments—also provides insights into the relationship between climate and megafaunal dynamics (*12*–*14*). For example, Pleistocene fossils of Beringia, the unglaciated landmass that connected present-day Yukon, Alaska, and northeastern Asia across the exposed Bering land bridge (Fig. 1A), reveals notably shifting patterns of habitat availability concurrent with climate swings. During the last cold period [35 to 16 thousand years before the present (kyr B.P.)], lower sea levels allowed dispersal into and out of North America via the exposed land bridge, although ice sheets limited movement southward into lower American latitudes (*15*). As the climate warmed (16 to 10 kyr B.P.), ice sheet melting opened the ice-free corridor to midcontinental America (*16*) and submerged the land bridge, forming the Bering Strait (*17*), which remains a barrier to the dispersal of terrestrial species [although examples of human-mediated exchanges seasonally and by sea are abundant in Iñupiaq and Dene' (Athabascan) oral traditions]. These changes altered habitat availability, connectivity, and food resources as cryoxeric steppe-tundra fragmented into boggy tundra, shrublands, wetlands, and boreal forests (*18*), which are less favorable habitats for some megafaunal species (*19*).

Despite substantial habitat changes in Beringia during Pleistocene climate cycles, the effects on megafaunal populations remain elusive (*13*, *14*). In this work, we combine geochemical and genomic analyses of horse fossils with traditional science to track changing habitats, population dynamics, and dispersal in Beringia from ~13 to >50 kyr B.P. Pleistocene horses offer a model to explore climate effects on megafauna, particularly in Beringia (*20*–*22*), where the *Equus* fossil record is exceptional (*23*). The Horse Nation and its movement and evolution are sacred to many Indigenous knowledge keepers in the Americas (*1*). Following the movement and evolution of the horse to reveal traditional knowledge fully aligns with many Indigenous scientific protocols. We thus integrate the biological signatures identified with Indigenous knowledge regarding ecosystem balance and sustainability to highlight the importance of corridors in safeguarding life.

Genomic, radiocarbon, and isotopic datasets

We applied Western and Lakota protocols to generate genomic data from 67 fossils originating in Beringia, Siberia, and continental North America (Fig. 1, A and B; fig. S1; and table S1). These data, which showed expected signatures of postmortem DNA damage (figs. S2 and S3) and limited error rates at transversion sites (fig. S4 and table S1), were compared with 158 genomes representing all known horse lineages (*24*–*26*) plus two donkeys (table S1). Additionally, we integrated genomic data with 200 radiocarbon dates and stable carbon and nitrogen isotope measurements ($\delta^{13}C$ and $\delta^{15}N$) from fossil horse collagen. To extend reconstruction of environmental conditions, dietary behavior, and habitats across the Northern Hemisphere, we prepared a database of 3809 $\delta^{13}C$ and $\delta^{15}N$ data from radiocarbon-dated Late Pleistocene megafauna (table S2). Combined, these data tracked habitat, diet, and genetic diversity changes across Beringia and beyond from ~13 to >50 kyr B.P.

Horses crossed Beringia multiple times

Phylogenetic analyses of mitochondrial and Y chromosome DNA suggest that horses crossed the Bering land bridge in both directions during the Pleistocene. Most horse fossils from North America cluster into two distinct major clades (Fig. 1C and figs. S5 and S6). The first ranged from south of the continental ice sheets (present-day US lower 48 states) to easternmost East Beringia via the ice-free corridor. Fossils from eastern Eurasia, including *Equus dalianensis* specimens from China (*27*) and South-East Russia near Vladivostok, appear sister to this clade at the mitochondrial level (Fig. 1C). Because *Equus* originated in North America (*28*), this phylogenetic structure supports dispersal into Eurasia beyond the limits of radiocarbon dating (i.e., >50 kyr B.P.). The second clade includes individuals from the

most western and northern extent of East Beringia (Fig. 1C and figs. S5 and S6) and clusters within broader Eurasian diversity, with closest relatives in northeastern Siberia, which supports migration back into America >46.8 kyr B.P.

Dispersals from Eurasia into North America

Analyses of genome-wide autosomal variation identified two major horse genetic lineages in North America. Principal components analysis (PCA) (Fig. 2A and figs. S7 to S9) and f3-outgroup statistics (fig. S10) showed strong differentiation between one cluster of specimens spanning easternmost East Beringia, the ice-free corridor, and south of the continental ice sheets, and a second cluster comprising the remaining American and Eurasian lineages. Within the latter, PC2 revealed a genetic cline stretching longitudinally from the Ural Mountains (≥15.4 kyr B.P.) to Alaska and northwestern Yukon (Fig. 2B) [Pearson correlation, adjusted coefficient of determination (R^2) = 0.941, $P < 2.2 \times 10^{-16}$]. Longitude was also correlated with the ADMIXTURE (*29*) component maximized in Alaskan individuals (adjusted R^2 = 0.949, $P < 2.2 \times 10^{-16}$) (fig. S11), all of which belonged to a highly supported monophyletic group, deriving from a larger Siberian cluster (Fig. 3, A and B, and fig. S12). These results support isolation-by-distance east of the Ural Mountains and across the Arctic into North America.

Temporal branching patterns within Alaskan and northwestern Yukon individuals support multiple dispersals across the Bering land bridge. Whereas a single dispersal event would produce a temporally sorted phylogenetic clade, no clear time structure emerged within Alaska (Fig. 3A), with the two most recent specimens (AV089 and AV096) branching off first. Their basal position is not a result of admixture with a divergent lineage because D-statistics and F4 ratio calculation (*30*) indicated significantly less genetic sharedness with the geographically closest, most divergent population from East Beringia versus with the other individuals from Alaska or northwestern Yukon (Fig. 3D and fig. S14). These results, alongside radiocarbon dating, support multiple independent dispersal events into North America from genetically close Siberian sources followed by limited genetic admixture (F4 ratios, 0.5 ± 0.3% to 6.1 ± 0.6%) with the other main American lineage.

Dispersals from North America into Eurasia

Several individuals deviated from the genetic cline linking the Eurasian and American Arctic (Fig. 2B and fig. S11). These included three >50–kyr B.P. specimens from northeastern Siberia (PH156, PH172, and R17x2), one ~23.6–kyr B.P. specimen from southwestern Siberia (Rus45), and two *E. dalianensis* specimens from more southerly latitudes (Fig. 1 and fig. S1). The latter showed ancestry from the lineage spanning easternmost East Beringia, the ice-free corridor, and south of the continental ice sheets, as revealed by ADMIXTURE (*29*) (1.3 ± 0.3% to 1.7 ± 0.2%; fig. S12 and table S1) and Struct-f4 (*31*) analyses (3.0 ± 0.3% to 3.6 ± 0.2%) (Fig. 3, B and C; fig. S14; and table S1). Similar ancestry was identified among the >50–kyr B.P. outliers from northeastern Siberia (0.8 to 1.7%), Rus45 (1.3%), and some Holocene (~3.9 to 4.7 kyr B.P.) remains from Iberia (2.3 to 4.2%; fig. S13 and table S1). F4 ratio analysis found 0.6 ± 0.2% to 0.7 ± 0.2% of such ancestry in two northeastern Siberian specimens dated to ~20.4 (PH147) and ~36.6 kyr B.P. (PH159) (Fig. 3D and table S1). Combined, these analyses support genetic contribution of North American horses to Eurasia before ~20.4 kyr B.P., extending from northeastern Siberia southward to the Russian Far East (*E. dalianensis*) and west to Iberia.

Understanding the frequency and limits of American horse dispersal across the Bering land bridge requires extensive genetic surveys of Pleistocene eastern Eurasia. Our findings reveal genetic exchanges across Beringia and well into Eurasia. This aligns with the movement patterns described within the sciences of the Iñupiaq and Dene' (Athabascan) (*2*) and with the Lakota and Syilx understanding of the evolution of their Peoples and the Horse Nation. Current labeling practices of Beringian fossils, influenced by geography and historical bias, overlook the dynamic history of species movement and reduce the multidimensionality of life forms. They ignore the Lakota mitakuye oyasin concept, which emphasizes "the relationality between life forms"—i.e., the interdependence between organisms, including microbes. We believe that the reliance on contemporary geographical labels, although convenient to Western paleontologists, has hindered constructive dialogs with Indigenous scientists.

Opening of the ice-free corridor

Beringia served as a dispersal corridor between Siberia and America until rising sea levels reformed the Bering Strait ~11 to 13 kyr B.P. (*17*). Meanwhile, the Laurentide and Cordilleran ice sheets coalesced from ~25 kyr B.P., depopulating Alberta until the ice-free corridor reopened ~13.8 ± 0.5 kyr B.P. (*16*) (Fig. 1B). The 19 horses analyzed from the Edmonton area, Alberta, lived ~13.1 kyr B.P., immediately after deglaciation (Fig. 1A and table S1). Although phylogenetically close, these horses diverged before the divergence of populations in easternmost East Beringia and those south of the continental ice sheets (Fig. 3A), which indicates that the ice-free corridor population did not emerge from either group expanding into the region.

To characterize the genetic source or sources entering the ice-free corridor, we performed population graph modeling with AdmixtureBayes (*32*) and OrientAGraph (*33*), considering key lineages in and around Beringia (Fig. 4 and figs. S15 and S16). These analyses confirmed the deep phylogenetic split within America between Alaska and/or northwestern Yukon and other regions, with the former receiving a minor genetic contribution from a source related to easternmost East Beringia (AdmixtureBayes, 3.0%; OrientAGraph, 2.5%). The genetic affinities linking the Ural Mountains to East Beringia, as well as the early divergence of the outlier northeastern Siberian and *E. daliensis* lineages, were also validated.

[1]Centre for Anthropobiology and Genomics of Toulouse, CNRS UMR 5288, Université de Toulouse, Toulouse, France. [2]Taku Skan Skan Wasakliyapi: Global Institute for Traditional Sciences, Keystone, SD, USA. [3]Oglala Lakota, Pine Ridge Reservation, SD, USA. [4]Department of Earth and Environmental Sciences, University of Ottawa, Ottawa, ON, Canada. [5]Department of Forestry and Natural Resources, Purdue University, West Lafayette, IN, USA. [6]Department of Biomolecular Engineering, University of California Santa Cruz, Santa Cruz, CA, USA. [7]Mt. Sanford Tribal Health Corporation, Hq Chistochina, AK, USA. [8]Ahtna Inc., ANCSA Regional Corporation, Slana, AK, USA. [9]Cheesh'Na Tribal Council, Gakona, AK, USA. [10]sqilxʷ/suknaqin or Okanagan Nation, Osoyoos Indian Band, Oliver, BC, Canada. [11]sqilxʷ/suknaqin or Okanagan Nation, snpink'tn Indian Band, Penticton, BC, Canada. [12]sqilxʷ/suknaqin or Okanagan Nation, Osoyoos Indian Band, Spetlumkn Oliver, BC, Canada. [13]Center for Cross-Cultural Studies, University of Alaska Fairbanks, Fairbanks, AK, USA. [14]Shageluk Tribe of Interior Alaska, Shageluk, AK, USA. [15]Institute of Culture and Environment, Alaska Pacific University, Anchorage, AK, USA. [16]Blackfoot Nation, Horse Spirit Healing and Wellness, McLean, SK, Canada. [17]Department of Ecology and Evolutionary Biology, University of California Santa Cruz, Santa Cruz, CA, USA. [18]Palaeobiology, Canadian Museum of Nature, Gatineau, QC, Canada. [19]Department of Earth Sciences and Biology, Carleton University, Ottawa, ON, Canada. [20]Smithsonian National Museum of Natural History, Washington, DC, USA. [21]Department of Earth System Science, University of California Irvine, Irvine, CA, USA. [22]Department of Archaeology, School of Geosciences, University of Aberdeen, Aberdeen, Scotland. [23]Genoscope, Institut de Biologie François Jacob, CEA, CNRS, Université d'Évry, Université Paris-Saclay, Évry, France. [24]Génomique Métabolique, Genoscope, Institut François Jacob, CEA, CNRS, Université d'Évry, Université Paris-Saclay, Évry, France. [25]Ice Age Museum, Shidlovskiy National Alliance "Ice Age," Moscow, Russia. [26]ArchaeoZOOlogy in Siberia and Central Asia – ZooSCAn, CNRS–IAET SB RAS International Research Laboratory, IRL 2013, Institute of Archaeology and Ethnography SB RAS, Novosibirsk, Russia. [27]Department of the Diversity and Evolution of Genomes, Institute of Molecular and Cellular Biology SB RAS, Novosibirsk, Russia. [28]Department of Archaeology, Ethnography and Museology, Altai State University, Barnaul, Russia. [29]Earth Sciences Department, Natural History Museum, London, UK. [30]University of Alaska Museum, Fairbanks, AK, USA. [31]Department of Geosciences, University of Alaska Fairbanks, Fairbanks, AK, USA. [32]Quaternary Palaeontology Program, Royal Alberta Museum, Edmonton, AB, Canada. [33]Department of Mammalogy, American Museum of Natural History, New York, NY, USA. [34]Institute of Arctic Biology, University of Alaska Fairbanks, Fairbanks, AK, USA. [35]Department of Earth and Atmospheric Sciences, University of Alberta, Edmonton, AB, Canada. [36]Alaska Stable Isotope Facility, University of Alaska Fairbanks, Fairbanks, AK, USA. [37]Department of Geosciences, University of Cincinnati, Cincinnati, OH, USA. [38]Department of Anthropology, University of Cincinnati, Cincinnati, OH, USA. [39]Government of Yukon, Palaeontology Program, Whitehorse, YT, Canada. ***Corresponding author. Email: runninghorse@takuskanskan.org (Y.R.H.C.); cbataill@uottawa.ca (C.P.B.); bashapir@ucsc.edu (B.S.); ludovic.orlando@univ-tlse3.fr (L.O.)**

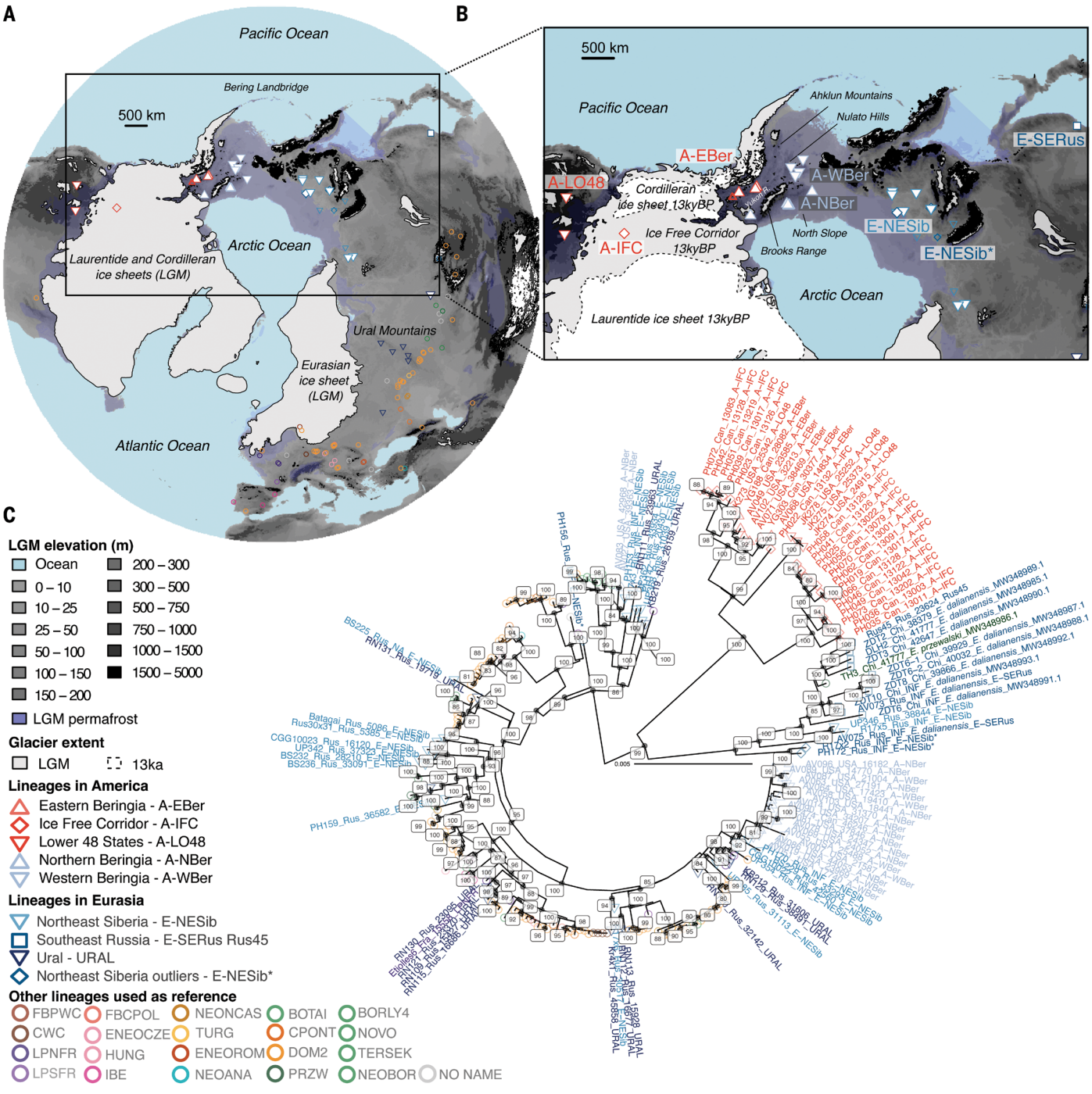

Fig. 1. Samples and mitochondrial phylogeny. (**A**) Sample location, with Last Glacial Maximum (LGM) geographic and climate features. LGM elevation and ocean extent were obtained by adding 130 m to the GEBCO 2014 bathymetric model (v20150318, http://www.gebco.net). LGM ice-sheet extent and permafrost are from Dalton *et al*. (*43*) and Lindgren *et al*. (*50*), respectively. Large, white-filled symbols indicate samples sequenced in this study, whereas small, open symbols indicate samples sequenced in previous studies. The colors of symbols reflect their main clusters of genetic affinities (table S1). (**B**) Inset zoom on Beringia and North America ~13 kyr B.P., showing key geographic features discussed in the main text. (**C**) Maximum likelihood (ML) tree for mitochondrial DNA manually rooted using a donkey outgroup, not shown ($N = 16{,}420$ base pairs, GTR+F+R10). Node supports (percentages) are displayed when greater than 80%, as estimated from 1000 replicates and ultrafast bootstrap approximation.

Graph models could not clearly resolve the history of the ice-free corridor population. AdmixtureBayes indicated early divergence (Fig. 4, A and B), whereas OrientAGraph grouped this population with easternmost East Beringia (Fig. 4C), suggesting that the ice-free corridor was primarily populated from north of the ice sheets. Both models showed significant contributions from deeply divergent groups—south of the continental ice sheets in AdmixtureBayes (5.0%) and easternmost East Beringia and the ice-free corridor in OrientAGraph (5.0% and 20.2%, respectively). This reflects a complex history of isolation and admixture during the earliest evolutionary stages, which remains unresolved without population-scale data from the deeper evolutionary past of America.

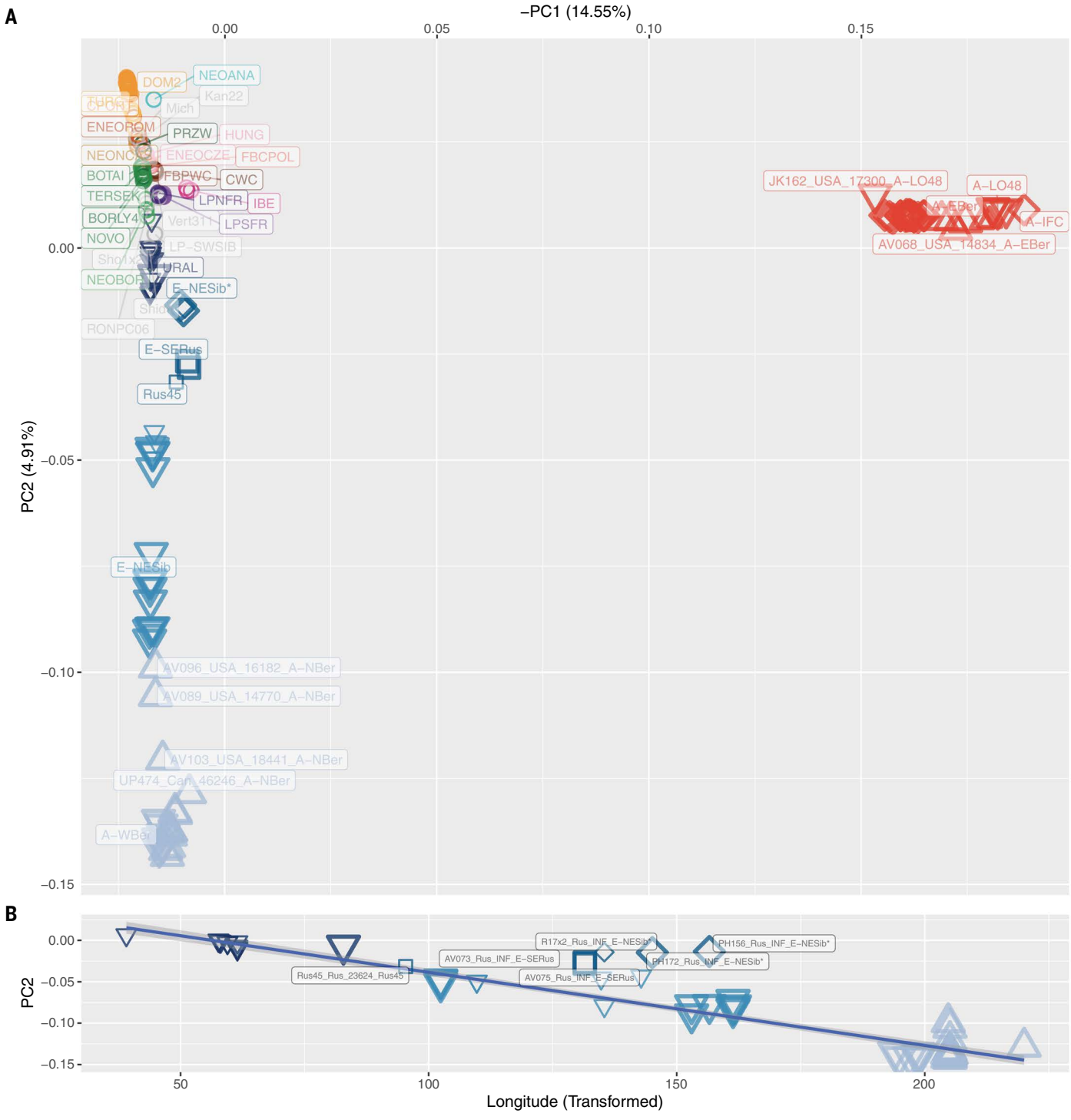

Fig. 2. Population structure. (**A**) PCA with percentages reflecting the variance proportions explained by PC1 and PC2. The AUTOSHRINK mode was applied, and a total of eight samples were projected on the PC space defined by the remaining samples. PC1 is reversed to mirror the geographic position of Eurasia and America in Fig. 1, A and B. Labels indicate the main lineages, except for a few notable samples. Newly sequenced samples are highlighted with larger sizes. (**B**) Linear regression of PC2 against longitude. The fitted Pearson linear regression model is shown with a blue line, with standard errors in gray. The labeled samples, including E-NESib*, E-SERus, and Rus45 individuals, were not included in the model because they are from different genetic backgrounds. Longitude was transformed by adding 360° when inferior to –30° to place the American continent in continuity with Eurasia.

Demographic modeling using GONE (*34*) revealed a brief population bottleneck (2.3-fold) 104 to 91 generations before ~13.1 kyr B.P. (~13,761 to 13,858 yr B.P.), aligning with the ice-free corridor opening (13.8 ± 0.5 kyr B.P.) (*16*) (Fig. 5A). We interpret this as the founder event of the ice-free corridor population, which maintained low effective sizes for 39 generations [91 to 52 generations; effective population size (N_e) = 2607] and collapsed further over 32 generations (52 to 20; N_e = 617) with no subsequent recovery (N_e = 842). These findings suggest that the ice-free corridor could not support substantial population growth at the time.

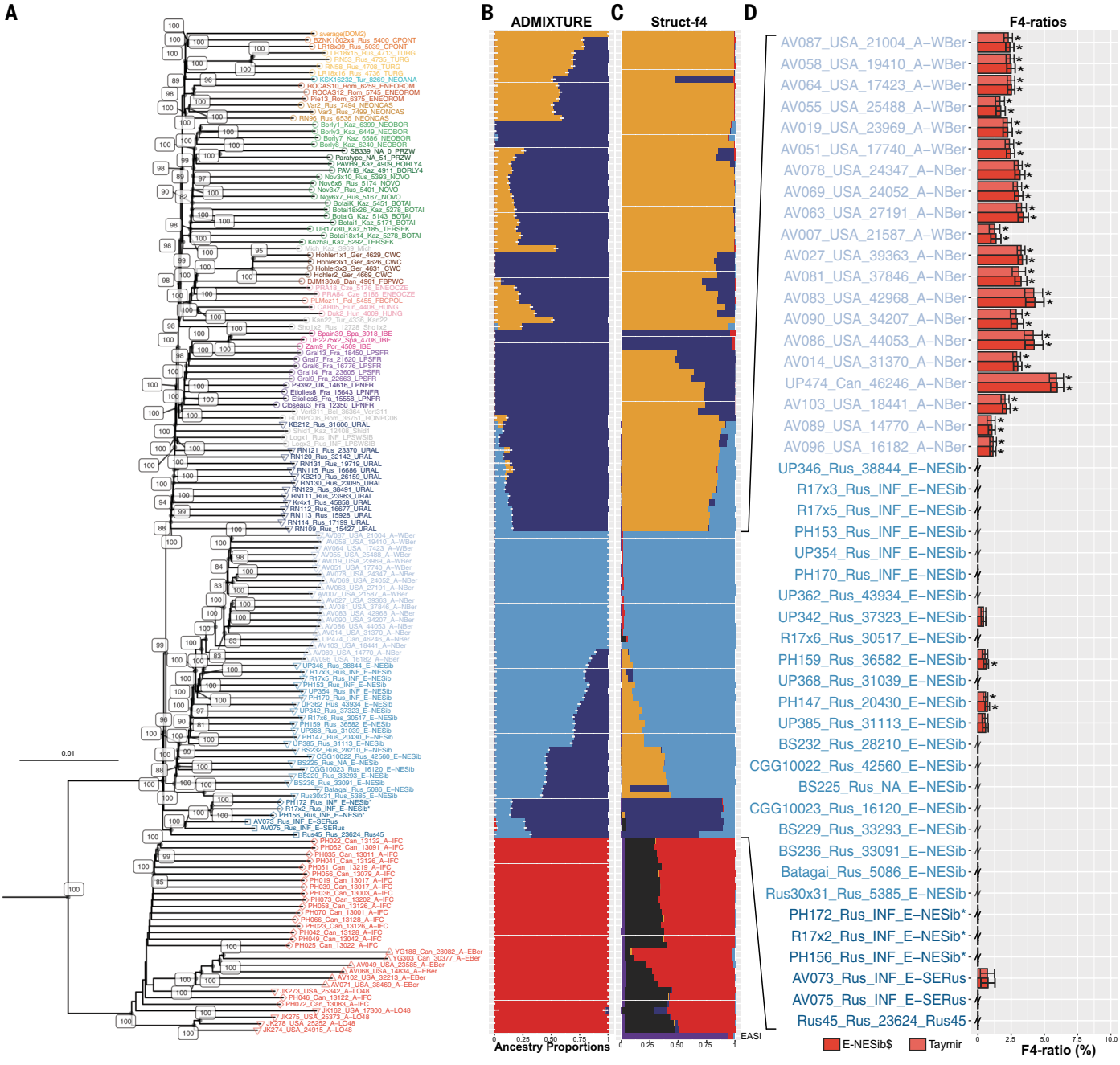

Fig. 3. Autosomal genetic affinities. (**A**) Neighbor-joining phylogeny for 9,386,235 autosomal transversion sites, with node supports estimated from 100 bootstrap pseudoreplicates. The DOM2 clade of modern domestic horses (*25*) shown at the top is collapsed, and the two donkeys used as outgroup are masked for clarity. (**B**) Genetic ancestry profiles from Admixture (*29*) ($K = 4$), with confidence range (white bars) estimated from 100 bootstrap pseudoreplicates. (**C**) Struct-f4 (*31*) profiles ($k = 6$), including EASI outgroup. (**D**) F4 ratio (*30*) estimates of A-EBer genetic ancestry in A-NBer, A-WBer, E-NESib, E-NESib*, E-SERus, and Rus45 horses. Estimates assume populations A-IFC or A-LO48 as the closest to the source of genetic ancestry native from America (A-EBer), and those E-NESib individuals from Taymir, or those devoid of A-EBer genetic ancestry (E-NESib$), as proxies for the northeastern Siberian source.

To explore the interplay between climate, habitat, and demography, we analyzed $\delta^{13}C$ and $\delta^{15}N$ values in megafaunal bone collagen from high latitudes (table S2) as proxies for diet, soil moisture conditions, habitat quality, and food availability (*19*). Ice-free corridor horses had extremely low $\delta^{15}N$ values (Fig. 5B) but $\delta^{13}C$ values typical of those of other Pleistocene horses (fig. S17), which indicates a consistent diet but exceptionally high soil moisture (*19*) associated with permafrost and glacial thaw (*16*). Replacement of cryoxeric steppe-tundra, which is ideal habitat for horses (*35*), by swampy tundra or forests reduced mobility, fragmented habitats, and limited food availability (*19*). Enamel hypoplasias indicate increased systemic stress—possibly nutrition related—at this time in North American horse populations (*36*). Our demographic modeling shows that the reduced carrying capacity of this environment constrained horse expansion in the ice-free corridor (Fig. 5A). A drop in $\delta^{15}N$ values occurred in other grazers between ~15 and 13 kyr B.P. in East Beringia (Fig. 5B) and beyond (fig. S18), a

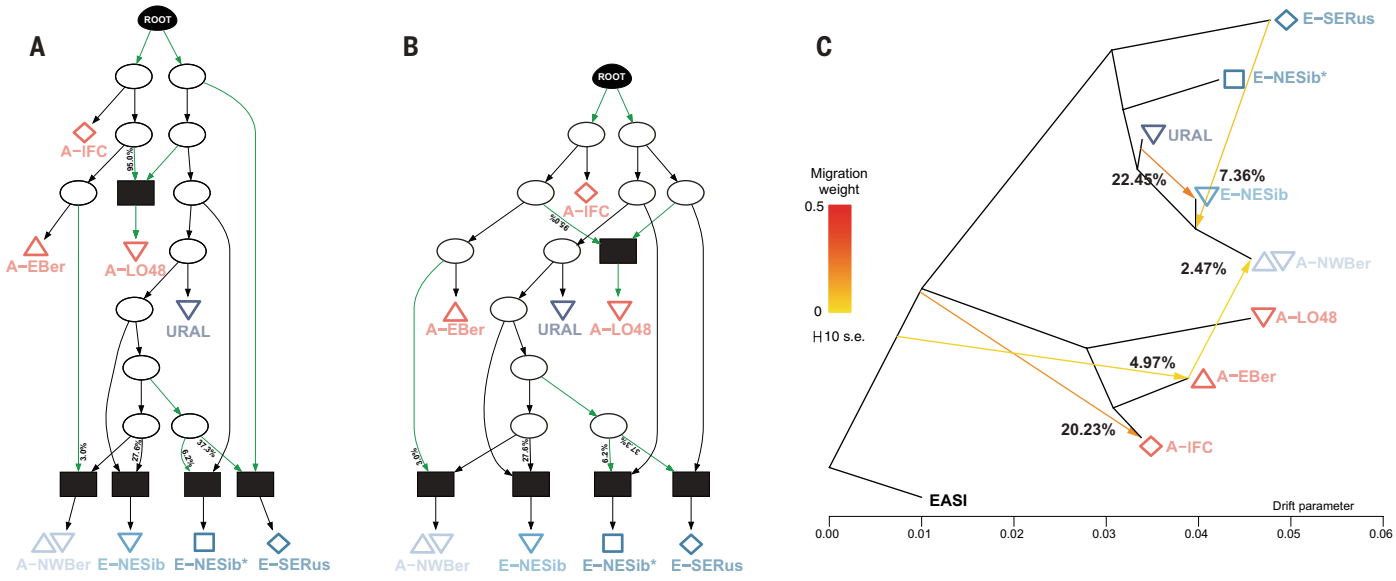

Fig. 4. Population graphs. (**A** and **B**) Two population graphs showing greatest posterior probability (36.7% and 22.6%, respectively) in AdmixtureBayes (*32*). Ancestral and admixture nodes are shown with circles and squares, respectively. Admixture proportions are shown in percentages. Branches substantially drifted are colored in green. The consensus graph and all other graphs accounting for ≥5% of the posterior graph distribution are shown in fig. S15, with drift and admixture estimates. Shapes and colors reflect the main genetic lineages investigated. (**C**) Best-supported graph model from OrientAGraph (*33*), considering $M = 5$ migration edges. Models considering up to five migration edges, and their residuals, are recapitulated in fig. S16.

phenomenon known as the Late Glacial Nitrogen Excursion (*19*). Loss of cryoxeric steppe-tundra because of climate warming and the resulting demographic impacts explain the decline in horse and other megafaunal grazer fossils at the Pleistocene-Holocene transition (*19*).

Discussion

This study extends previous paleogenomic research (*22*, *25*, *37*–*39*) reporting an extensive diversity of late Pleistocene horse lineages that contrasts sharply with horse diversity today. Deeply divergent lineages in Eurasia and North America suggest strong geographic and environmental barriers isolating populations during Pleistocene climate cycles (*40*). Despite this, multiple dispersals between continents occurred during favorable glacial conditions. The genetic cline linking the Eurasian Arctic and Alaska indicates that the cryoxeric steppe-tundra defining the "mammoth steppe" (*41*, *42*) provided a favorable dispersal corridor ranging across the Bering land bridge. However, this transcontinental cline barely extended into America, as northwestern Alaskan populations were predominantly Eurasian genetically (93.7 to 99.5%), whereas northeastern Siberian populations had minimal eastern Beringian ancestry (≤0.8 ± 0.2%). Natural barriers, such as the Ahklun Mountains, Nulato Hills, and Brooks Range, considerably limited, but did not entirely prevent, horse dispersal between ~14.8 and 46.2 kyr B.P. (*43*).

Northeastern Siberian horses from ~5.1 to >48.4 kyr B.P. largely lacked American ancestry, but earlier dispersal(s) from eastern Beringia left lasting genomic footprints in Eurasia, such as in the Russian Far East >50 kyr B.P. (*E. dalianensis*) and Holocene Iberia (Fig. 3C). Struct-f4 and population graph modeling placed these dispersals beyond the limits of radiocarbon dating, aligning with a divergence of at least 285 kyr B.P. between Holocene Iberian and other Eurasian lineages (*38*). Horses near the Ural Mountains strongly influenced the genomic makeup of Eurasian horses: They group basally to most late Pleistocene and Holocene lineages in Anatolia, Central Asia, and Europe (Fig. 3A) and were part of a genetic cline connecting Arctic Eurasia and America. This lineage likely extended farther east than the Urals, as evidenced by the ~45.8–kyr B.P. Kr4x1 specimen from southwestern Siberia near Novosibirsk. Their range likely shifted with time and climate because their genetic sharedness with the ~5.1–kyr B.P. Batagai sample from northeastern Siberia (*39*) was unprecedented in older Siberian specimens (fig. S14).

Further east than Alaska and northwestern Yukon, populations north and south of the continental ice sheets formed distinct genetic subgroups, supporting the role of glacial-interglacial cycles in driving megafauna population dynamics (*20*, *44*). Horses entered the ice-free corridor after the ice sheets retreated but did not expand, likely owing to unfavorable conditions. As permafrost thawed and glaciers retreated ~12 to 15 kyr B.P. (*19*), high soil moisture in deglaciated areas (indicated by $\delta^{15}N$ data) hindered the formation of cryoxeric steppe-tundra crucial for horses. Moist environments replaced the mammoth steppe-tundra with swampy tundra and boreal forest dominated by woody, grazing-resistant plants (*18*, *19*), which in turn resulted in reduced mobility (*45*) and demographic decline (*46*) of large grazers. By contrast, mixed feeders and browsers, such as wapiti and moose, thrived and expanded their ranges (*19*, *47*, *48*). These observations align with the Lakota mitakuye oyasin scientific principle (*1*), which defines a species' habitat by its relationality with other life forms essential for its survival rather than by geography. As climate shifts affect the life forms that each species needs to thrive, their need to exist within their relational habitat serves as the driving force for movement or migration.

Permafrost is projected to largely disappear within a century (*49*), replicating conditions in Alberta ~13 kyr B.P. across much of the Arctic, with severe implications for life. The global loss of the circumpolar permafrost-tundra belt, creating environments less favorable to movement, may also challenge de-extinction prospects for the megafauna grazers that roamed the high latitudes during the late Pleistocene (*8*).

Chief Harold Left Heron, a traditional scientist, Elder, and knowledge keeper for the Lakota Peoples, offers the following perspective: "We understand individual bodies as balanced ecosystems hosting a diversity of life forms, including microbial, all aligned towards health. When survival becomes challenging, life forms whose relationality is being affected utilize ouŋye (most closely translated in English as 'agency') to reach out to other related but different forms

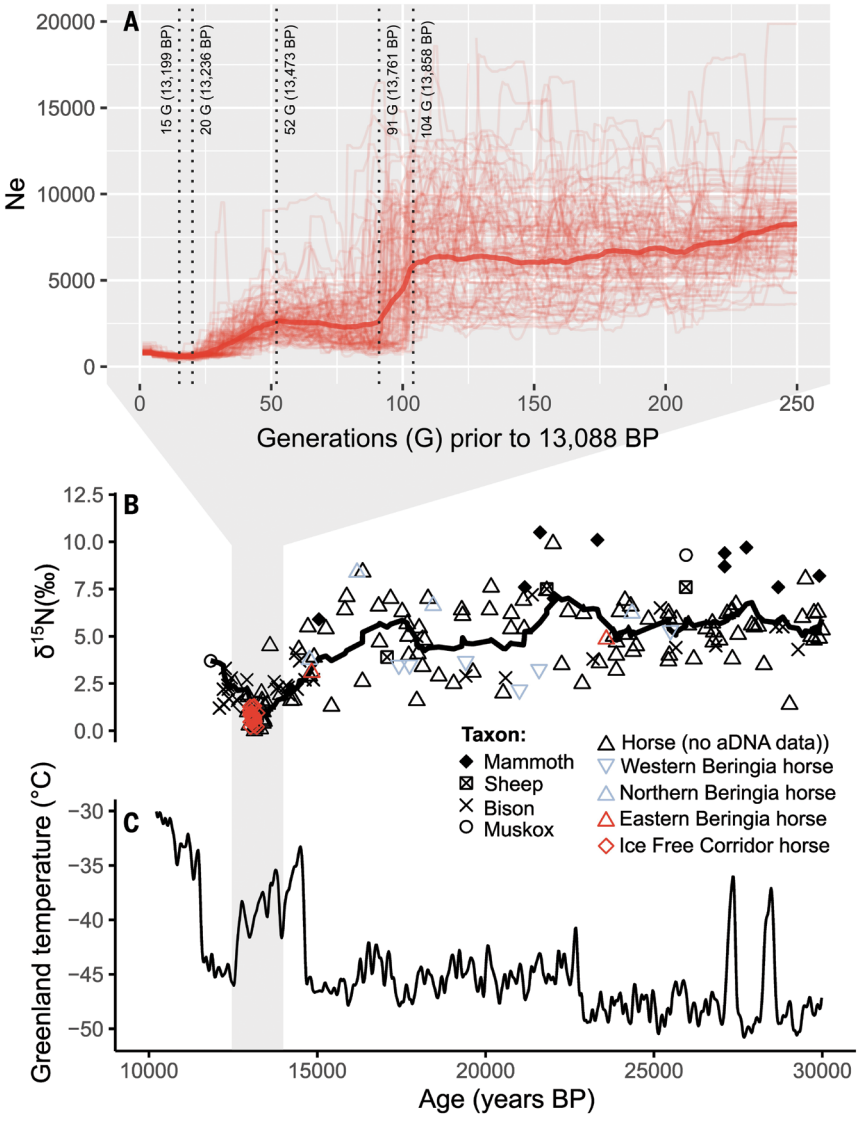

Fig. 5. Demographic and isotopic profiles of the ~13–kyr B.P. A-IFC population from Alberta, Canada. (**A**) GONE (*34*) demographic trajectory, with confidence intervals estimated from 100 bootstrap pseudoreplicates. Dashed vertical lines delineate time periods with changing demographic regimes. Time is shown in numbers of generations ("G") relative to the A-IFC population (bottom *x* axis). An equivalence in calibrated B.P. years is provided between parentheses, considering the average calibrated B.P. radiocarbon date of the specimens (i.e., 13,088 yr B.P.) and the average generation time from (*25*) (i.e., 7.4 years). (**B**) Time series of stable nitrogen isotope values in bone collagen of East Beringia megafauna (table S2) and temperature record for Greenland (*51*). The curves represent the average in sliding windows of 10 samples, with shapes according to common name. Data compiled from the literature or generated in this work are shown with black and colored symbols, respectively. (**C**) Greenland temperature variation between 10 and 30 kyr B.P. [data from (*51*)]. aDNA, ancient DNA.

of life to preserve sustainability. Joining improves their ability not just to survive, but to thrive. This process is called yutaŋ'kil and it combines and diversifies life genetically to ensure an ebb and flow by adjusting and responding to changing conditions. As Lakota, we acknowledge this with each breath." He further explains that respecting the inherent need for life forms to freely move within their optimal relational home provides the ideal conditions for sustainability. Therefore, attempts to preserve megafauna species as they were genetically at one specific point in time disregards this complex diversity of alliances with other life forms and is unlikely to strengthen sustainability. Conversely, ensuring the movement of life through physical corridors connecting a diversity of habitats allows life to adapt and survive in changing environmental conditions.

Wilson Justin is an Upper Ahtna/Upper Tanana Dene' (Athabascan) Elder and knowledge keeper of the Alth'setnay clan, born at Nabesna, Alaska. Addressing the movement inherent in all life and the scope of his People's world, he recalls a well-traveled, physical pathway referred to as the "Medicine Man Trail," which ensured diversity and sustainability for many thousands of years. The Trail reaches from Alaska, across Siberia into Mongolia, but also through Canada, across Lakota territory, and into Maya territory, branching off throughout. "Traveling the trail as far as the horizon could be seen introduced us to a diversity of life forms in constant motion. We learned the way natural systems work and how all life is interconnected and interdependent. This knowledge is held in our songs, stories and in the sciences and life ways we carry. Whether human, horse or the microbial life that moves with them, singing the song of life is a gift that ensures sustainability."

Jane Stelkia is an Elder for the sqilxʷ/suknaqin or Okanagan Nation, which is based on her People's traditional lands in Canada. As a native Nsyilxcen speaker and a keeper of traditional science surrounding Snklc'askaxa, the Horse Nation, she confirms her People's experience with the "Medicine Man Trail" and adds: "Snklc'askaxa serve as balancers in the ecosystem, and when we Indians are in the mountains on Snklc'askaxa, we connect with the water, the rain, the trees, the flowers blooming. Together we experience all of life. Today, we live in a world where the boundaries and obstacles created by mankind do not serve the majority of life. In this study, Snklc'askaxa is offering us medicine by reminding us of the path all life takes together to survive and thrive. It is time that humans help life find the openings and points to cross and move safely."

The ability for life forms to migrate as relationality around them changes is key for long-term survival. Genetic change as a result of yutaŋ'kil should not be feared or artificially blocked but respected as proof of life's strength and resilience. Our ability and willingness to support this process determines our sustainable future.

REFERENCES AND NOTES

1. M. Hunska Tašunke Icu *et al.*, "Standing for *Unči Maka* (Grandmother Earth) and All Life: An Introduction to Lakota Traditional Sciences, Principles and Protocols and the Birth of a New Era of Scientific Collaboration" (Maxwell Museum Technical Series, no. 42, 2023).
2. W. A. Oquilluk, L. L. Bland, *People of Kauwerak: Legends of the Northern Eskimo* (AMU Press, 1973).
3. F. A. Smith *et al.*, *Proc. Natl. Acad. Sci. U.S.A.* **119**, e2115015119 (2022).
4. Y. Malhi *et al.*, *Proc. Natl. Acad. Sci. U.S.A.* **113**, 838–846 (2016).
5. E. J. Lundgren *et al.*, *Science* **383**, 531–537 (2024).
6. P. Jaureguiberry *et al.*, *Sci. Adv.* **8**, eabm9982 (2022).
7. J. Huang *et al.*, *Nat. Clim. Chang.* **7**, 875–879 (2017).
8. M. Macias-Fauria, P. Jepson, N. Zimov, Y. Malhi, *Phil. Trans. R. Soc. B* **375**, 20190122 (2020).
9. W. J. Ripple *et al.*, *Bioscience* **67**, 197–200 (2017).
10. R. E. Morlan, J. Cinq-Mars, in *Paleoecology of Beringia*, D. M. Hopkins, J. V. Matthews, C. E. Schweger, S. B. Young, Eds. (Academic Press, 1982), pp. 353–381.
11. E. Y. Pavlova, V. V. Pitulko, *Quat. Int.* **549**, 5–25 (2020).
12. J. A. Swift *et al.*, *Bioscience* **69**, 877–887 (2019).

13. D. H. Mann *et al.*, *Proc. Natl. Acad. Sci. U.S.A.* **112**, 14301–14306 (2015).
14. M. Stewart, W. C. Carleton, H. S. Groucutt, *Nat. Commun.* **12**, 965 (2021).
15. E. J. Gowan *et al.*, *Nat. Commun.* **12**, 1199 (2021).
16. C. D. Clark *et al.*, *Boreas* **51**, 699–758 (2022).
17. J. R. Farmer *et al.*, *Proc. Natl. Acad. Sci. U.S.A.* **120**, e2206742119 (2023).
18. J. W. Williams, B. N. Shuman, T. Webb III, P. J. Bartlein, P. L. Leduc, *Ecol. Monogr.* **74**, 309–334 (2004).
19. M. T. Rabanus-Wallace *et al.*, *Nat. Ecol. Evol.* **1**, 0125 (2017).
20. E. D. Lorenzen *et al.*, *Nature* **479**, 359–364 (2011).
21. P. D. Heintzman *et al.*, *eLife* **6**, e29944 (2017).
22. A. O. Vershinina *et al.*, *Mol. Ecol.* **30**, 6144–6161 (2021).
23. C. R. Harington, *Quat. Sci. Rev.* **30**, 2341–2354 (2011).
24. L. Orlando, *Annu. Rev. Genet.* **54**, 563–581 (2020).
25. P. Librado *et al.*, *Nature* **631**, 819–825 (2024).
26. W. T. T. Taylor *et al.*, *Science* **379**, 1316–1323 (2023).
27. J. Yuan *et al.*, *Quat. Sci. Rev.* **250**, 106691 (2020).
28. B. J. MacFadden, O. Carranza-Castañeda, *Bull. Fla. Mus. Nat. Hist.* **43**, 163–185 (2002).
29. D. H. Alexander, J. Novembre, K. Lange, *Genome Res.* **19**, 1655–1664 (2009).
30. N. Patterson *et al.*, *Genetics* **192**, 1065–1093 (2012).
31. P. Librado, L. Orlando, *Bioinformatics* **38**, 2070–2071 (2022).
32. S. V. Nielsen *et al.*, *PLOS Genet.* **19**, e1010410 (2023).
33. E. K. Molloy, A. Durvasula, S. Sankararaman, *Bioinformatics* **37**, i142–i150 (2021).
34. E. Santiago *et al.*, *Mol. Biol. Evol.* **37**, 3642–3653 (2020).
35. G. M. MacDonald, T. K. McLeod, *Quat. Int.* **32**, 87–95 (1996).
36. C. I. Barrón-Ortiz, C. N. Jass, R. Barrón-Corvera, J. Austen, J. M. Theodor, *Paleobiology* **45**, 484–515 (2019).
37. M. Schubert *et al.*, *Proc. Natl. Acad. Sci. U.S.A.* **111**, E5661–E5669 (2014).
38. A. Fages *et al.*, *Cell* **177**, 1419–1435.e31 (2019).
39. P. Librado *et al.*, *Proc. Natl. Acad. Sci. U.S.A.* **112**, E6889–E6897 (2015).
40. D. Froese *et al.*, *Proc. Natl. Acad. Sci. U.S.A.* **114**, 3457–3462 (2017).
41. R. D. Guthrie, *Frozen Fauna of the Mammoth Steppe: The Story of Blue Babe* (Univ. Chicago Press, 1990).
42. S. A. Zimov, N. S. Zimov, A. N. Tikhonov, F. S. Chapin III, *Quat. Sci. Rev.* **57**, 26–45 (2012).
43. A. S. Dalton *et al.*, *Quat. Sci. Rev.* **321**, 108345 (2023).
44. P. F. Campos *et al.*, *Proc. Natl. Acad. Sci. U.S.A.* **107**, 5675–5680 (2010).
45. A. G. Rowe *et al.*, *Sci. Adv.* **10**, eadk0818 (2024).
46. A. D. Barnosky, P. L. Koch, R. S. Feranec, S. L. Wing, A. B. Shabel, *Science* **306**, 70–75 (2004).
47. M. Meiri *et al.*, *Proc. R. Soc. B* **281**, 20132167 (2014).
48. M. Meiri, A. Lister, P. Kosintsev, G. Zazula, I. Barnes, *J. Biogeogr.* **47**, 2223–2234 (2020).
49. D. Guo *et al.*, *Proc. Natl. Acad. Sci. U.S.A.* **120**, e2301954120 (2023).
50. A. Lindgren, G. Hugelius, P. Kuhry, T. R. Christensen, J. Vandenberghe, *Permafrost Periglac. Process.* **27**, 6–16 (2016).
51. P. Kindler *et al.*, *Clim. Past* **10**, 887–902 (2014).
52. C. Bataille, L. Orlando, Following Late Pleistocene horse migration toward our sustainable future, Open Science Framework (2025). https://doi.org/10.17605/OSF.IO/Z2XT4

ACKNOWLEDGMENTS

We thank the Vuntut Gwitchin and Tr'ondëk Hwëch'in for enabling research on Yukon fossils collected from within their Traditional Territories. This research and all Indigenous scientific contributions were conducted under the formal Indigenous Review Board (IRB) process put in place by Oglala Lakota Elder traditional government representatives on the Board of Taku Skan Skan Wasakliyapi: Global Institute for Traditional Sciences (GIFTS), joined by their counterparts in the Iñupiaq, Dene' (Athabascan), Blackfoot, and sqilx^{w}/suknaqin or Okanagan Nation. Wopila Tanka to Sam High Crane (Wapageya Mani) for his vision and leadership and to Šungwakaŋ, the Horse Nation, for their collaboration and for continuing to show us the way. **Funding:** Y.R.H.C. was supported by the European Union's Horizon 2020 research and innovation program under the Marie Skłodowska-Curie (grant agreement890702-MethylRIDE). C.P.B. was supported by the NSERC Discovery Grant RGPIN-2019-05709, the New Frontiers in Research Fund Exploration NFRFE-2023-00365, and by the Visiting Professor scholarship 2023 at Université Paul Sabatier (Université de Toulouse). A.H. was supported by UKRI MSCA guarantee fund (PleistoDem, EP/X023249/1). J.H.M. was supported by National Science Foundation (NSF) grant DEB-2135479. This work was supported by France Génomique National infrastructure, funded as part of the "Investissement d'avenir" program managed by Agence Nationale pour la Recherche (ANR-10-INBS-09); the France Génomique Appel à Grand Projet (ANR-10-INBS-09-08, BUCEPHALE and MARENGO projects); the CNRS International Research Project AnimalFarm; the TIRIS "Scaling-Up Science Program" BasicExtinct from the Université de Toulouse; and ERC under the European Union's Horizon 2020 research and innovation program (grant agreements 681605-PEGASUS and 101071707-HorsePower). **Author contributions:** Bioinformatics: L.O., with input from Y.R.H.C.; Databasing: C.P.B., Z.L., D.F., E.L., P.D., C.N.J., C.I.B.-O., D.M., M.W., J.H.M., G.Z.; First Nations protocols: Y.R.H.C., Chief J.A.H., Chief H.L.H.; Funding acquisition: Y.R.H.C., C.P.B., A.H., J.H.M., B.S., L.O.; Material, reagents, and infrastructure: C.P.B., B.C., A.P., P.H.O., J.-M.A., P.W., I.V.K., S.K.V., M.A.K., A.S.G., A.A.T., I.B., P.D., C.N.J., R.D.E.M., P.G., D.M., D.G.F., G.Z., B.S., L.O.; Molecular investigations: Y.R.H.C., S.H., J.D.K., L.C., G.T., L.T.-C., S.S., A.S.-O., M.A.K., with input from L.O.; Radiocarbon dating: J.S.; Study coordination: Y.R.H.C., L.O.; Study design: Y.R.H.C., C.P.B., Chief J.A.H., B.S., L.O.; Supervision: Y.R.H.C., C.P.B., B.S., L.O.; Visualization: Y.R.H.C., C.P.B., L.O.; Writing – original draft: Y.R.H.C., C.P.B., L.O.; Writing – review & editing: all coauthors. **Diversity, equity, ethics, and inclusion:** In part, this study was designed to communicate knowledge that is part of the Indigenous scientific base regarding how to sustain life. Anything not expressly published is being kept under the guardianship of traditional knowledge protocols consistent with those of the Indigenous coauthors. The traditional IRB process that enabled this study served as an umbrella for all aspects of research. Although the Lakota initiated this project, they did so after consultation with Indigenous leaders, knowledge keepers, and scholars from other Nations whose traditional lands were the source of many of the life samples analyzed. The participants from other Indigenous Nations expressly requested coverage under this IRB owing to its comprehensive approach. Under this Lakota-designed IRB process, the outcome of this research could not have been published if the process undertaken had not met all Indigenous scientific protocols at issue. The leading author of this study joined the genomics team at CAGT (France), expressly at the request of Lakota community leaders to conduct this research in collaboration and to aid in establishing new protocols for future cross-cultural scientific collaborations involving Indigenous Peoples, the life forms they protect, and traditional knowledge and sciences. The IRB leadership became coauthors to express their level of responsibility, contribution, and engagement at each stage of the process. Extensive travel between France and Lakota territory occurred for in-person meetings and cross-cultural exchange. This included laboratory facility visits, discussion and interpretation of results, and ceremonial participation. Each of these leaders represented community members and groups with specific interest in the research outcomes. As is aligned with Lakota protocols, representatives from the Indigenous Nations whose territories are covered in this research were consulted and invited to join this study. In-person meetings with these knowledge keepers and scientists took place in their respective territories, and their scientific contributions were included in a manner aligned with their protocols. **Competing interests:** B.S. is the chief science officer at Colossal Biosciences, a company working on de-extinction. The authors declare no other competing interests. **Data and materials availability:** In agreement to all stakeholders of this study, the sequence data generated are available for download at the European Nucleotide Archive (accession no. PRJEB74327). The radiocarbon dates and isotopic data generated in this study are provided in table S1, with reference to their official experimental code. The compiled database of radiocarbon dates and isotopic data is provided in table S2 and is available on the Open Science Framework (*52*) together with the matrix of autosomal transversion variation, mitochondrial, and Y chromosomal sequence alignments.

SUPPLEMENTARY MATERIALS

science.org/doi/10.1126/science.adr2355
Materials and Methods; Figs. S1 to S18; Tables S1 and S2; References (*53*–*83*); MDAR Reproducibility Checklist

Submitted 21 June 2024; accepted 19 March 2025

10.1126/science.adr2355

Science
AAAS

Supplementary Materials for

Sustainability insights from Late Pleistocene climate change and horse migration patterns

Yvette Running Horse Collin (Tašunke Iyanke Wiŋ) *et al*.

Corresponding authors: Yvette Running Horse Collin (Tašunke Iyanke Wiŋ), runninghorse@takuskanskan.org;
Clément P. Bataille, cbataill@uottawa.ca; Beth Shapiro, bashapir@ucsc.edu;
Ludovic Orlando, ludovic.orlando@univ-tlse3.fr

Science **388**, 748 (2025)
DOI: 10.1126/science.adr2355

The PDF file includes:

Other Supplementary Material for this manuscript includes the following:

Materials and Methods

Applied Lakota Genomic Scientific Protocols

All Lakota science protocols begin with the application of their ethical and multidimensional construct. As maintaining sustainability between life forms is their scientific goal, the application of this construct is mandatory within all research to ensure that *(i)* as little harm as possible is done to life, *(ii)* maximum alignment of natural forces occurs, and *(iii)* optimal genomic data can be obtained for the specific scientific purpose determined. There are no direct translations from the Lakota language into English. Therefore, this protocol is brought forward first in the Lakota language, as would be directly understandable and applicable to a Lakota traditional science practitioner, and then described in English, with specific Lakota scientific concepts utilized when precise English translation is not possible. This protocol outlines the steps necessary to set the boundaries of this construct, including the application of their Seven Generations Analysis *(1),* which is applied at the completion of every study to evaluate the impact of the research findings on the next seven generations of life and beyond. This construct and related principles were applied throughout this study. They are additive to the Western scientific genome sequencing protocol described below in the next section.

Woksape wamahatuye woableza woecun kin iyuha wakaŋ ya unkowanpi, wičoni wakan yelo.
Woyucaŋ lena ohinniyaŋ wočiccumptan il unhapikte.
Oyate ta woecun kiŋ wokunze ai kwake.
Wakaŋ tanka ta woyake oyate oun kin le kiyela awica upi okihi.
Wopasi kin taku oyate ecetkiya akipa yuha kte, waste na sica? Toske Unči Maka na Wamakanska ahiglye kte sel?
Tuwe icunkte kin ota kin šungwakaŋ woslolye yuha kte.
Sungwakaŋ otakuye opapikte wopasi ki canke' "Yuoniha" wicakichopi kte.
Sunwakaŋ naği tawapi ki lena nahangci ni pi heun "piitchiyapi hel ogna kecanwicunyampi"
Mni wanca kowakata oyate tuwe sunka wakan yuonihapi kin hena ilag wicun yanpi kte. Ho hecel sunka wakan hena wicotawacin ikpazo yunkapi kte.
Wopasi kin taku hecena Wiconi pi can hogna ilagwicunpi kta heca
Wičoni kin topa opa lo: Taku; oniyaŋ; naği; otakuye.
Lena iyuha hecel wopasi ecunpi kte
Sunkwakan nagi ki chopi canke' wounspe' tawapi ki wicakilapikte hecel taku sloye' necinyapi ke henna yunayeniciyapi okihipi.
Wowasi kin wicoincaga Šakowiŋ tokatakiya icanupi hecel woecun iglustanpi kin iyowaza onagu iyapi kte
Wasiču Wakanyapi wamahituya wounspe akiyapi na naği kicunya woableza ki lena iyastag ecumpihantansh ecila Wicoincaga Šakowiŋ win Tokatakiya woableza lena yuha pi kte.

In practice, and for conducting genomic work, this protocol is divided into four parts.

The first step (Laboratory Preparation) involves cleaning the laboratory space and all spaces utilized in the experiment of any interfering taku particles (matter), oniyaŋ (energy or force), or naği (essence of life) that would influence the experiment in an adverse fashion, or reduce the efficacy of the outcomes (see reference (1) for more detailed explanation of Lakota scientific terms).

The second step (Sample Preparation) applies the same cleaning process to samples, as it is critical that the ouŋye (agency) of each of the life forms attached to the samples is acknowledged. Extreme attention should be paid to which groups of samples are included in a given experimental session, to ensure that their mitakuye (relationality) is respected and to maximize the desired outcome.

The third step (Strengthening and Holding Forces Together) is necessary throughout the experimental work and requires maximizing the alignment of the practitioner with the sample naği, škaŋ (life flow), mitakuye, and ouŋye, throughout the process. This establishes the necessary order for different components of life to return in each of its parts to the samples during the experimental period, ensuring that measurement can be optimally recorded.

The last step (Dissipation) guides the end of the experiment to allow for the respectful dissipation of each of the components and forces utilized according to the speed at which the ouŋye and physics of the specimens allow and require.

Genome sequencing

A total of 66 ancient horse skeletal and dental remains were processed in the ancient DNA facilities of the Centre for Anthropobiology and Genomics of Toulouse (CAGT, France). The experimental procedure follows methodologies previously described *(25,53,54)*, and relies on seven sequential technical operations, carried out between the third and fourth steps described above. These include: (1) sample powdering (80-1,080 mg, median=200 mg); (2) powder decontamination with bleach (15 min in 4mL of a 0.5% sodium hypochlorite solution, followed by 3 consecutive water washes), pre-digestion, and digestion; (3) DNA purification; (4) USER© enzymatic treatment; (5) DNA library construction; (6) PCR amplification, and; (7) DNA library pooling and sequencing.

The pre-digestion step involved incubating the bone and/or dental powder with 3.85 mL of digestion buffer (0.45M EDTA, 0.25mg/mL Proteinase K (ThermoFischer Scientific), and 0.5% N-LaurylSarcosyl (Dutscher) for 60 mins at 42°C, before retrieving undigested pellets by removing the supernatant following a 2 minute centrifugation at maximal speed, and completing digestion overnight in 3.85 mL of fresh digestion buffer with agitation at 37°C. DNA purification was carried out by reducing the volume of the digestion reaction to approximately ~250 uL, first by using a 45-90 min centrifugation at 3,000 rpm on a Centricon column (Millipore 30 kDa), and then by using MinElute columns (QIAgen), with a final eluate of 60 uL. Triple indexed DNA libraries were constructed following end-repair, adapter ligation and nick filling reactions, following enzymatic treatment of 22.8 uL of purified DNA extract with 7.0 uL of USER (New England Biolabs) enzymatic mix for 3 hours at 37°C *(38,54)*. The size profile and DNA concentration of each individual library was checked using the High Sensitivity DNA Screen Tape system on a TapeStation 4200 instrument (Agilent). DNA libraries were pooled before sequencing on a MiniSeq Illumina instrument at CAGT for assessing DNA content and preservation levels (Paired-end mode, 2x81 cycles), and HiSeq 4000 and/or NovaSeq 6000/X Illumina instruments for deep shotgun sequencing in the dedicated facilities of Genoscope (Evry, France; Paired-end mode, 2x75 cycles) and Novogene (Cambridge, UK; 2x150 cycles), respectively.

Fifteen of the 67 newly processed horse samples were treated in a dedicated ancient DNA facility at the University of California Santa Cruz Paleogenomics Laboratory (UCSC PGL; table S1). For each of these, 50 mg of bone powder was pretreated with sodium hypochlorite in accordance with Korlević and Meyer (*55),* followed by the DNA extraction protocol described in

(56). Each extract was prepared into single-stranded DNA libraries using the Santa Cruz Reactions method *(57).* Each DNA library was enriched for 22,619 genomic regions spanning the horse genome, as described in *(58).* Custom Arbor myBaits (detailed in *(58))* were used on all individual libraries. The enriched regions targeted neutral single nucleotide polymorphisms (SNPs) ascertained from four ancient horse genomes previously sequenced to 18-26X coverage: two from North America (YG303.325 and YG188.42/YT03-40; *(22)*) and two from Siberia (Batagai; *(39),* and CGG10022 *(37, 59);* table S1). SNP ascertainment and comparison of the two capture methods are described in detail in *(58).* All 15 capture libraries were sequenced on Illumina NextSeq 550 (2x150 cycles) or NextSeq 2000 (2x61 cycles) instruments. Four of the fifteen specimens processed at UCSC through target enrichment were also shotgun sequenced at CAGT to maximize genome coverage (JK273 (KU42626), JK274 (KU43413), JK275 (KU47538) and JK278 (KU47519); table S1).

Read processing, mapping and sequence variation

Paired-end FASTQ sequencing reads were demultiplexed and trimmed for low-quality ends and adapters, using AdapterRemoval2 (v2.3.1), using the high-sensitivity parameters from *(60),* and tolerating one mismatch in each of the 7 bp internal indexes (--trimns --trimqualities --minadapteroverlap 3 --mm 5). This procedure returned read pairs showing sufficient sequence overlap for being collapsed in single reads (*'Collapsed*' and '*Collapsed truncated*'), as well as the remaining fraction of read pairs showing no significant overlap ('*Paired'*). Both types of reads were aligned against the horse EquCab3 reference genome *(61),* supplemented with the Y-chromosome contigs from *(62),* disregarding those shorter than 25 nucleotides. Paleomix (v1.2.13; *(63))* was used post-trimming/collapsing, including for read alignment using Bowtie2 (v2.3.4.1; *(64))* with the parameters recommended by Poullet & Orlando *(65),* local read realignment around indels using GATK (v3.8.1; *(66)),* and the filtering of duplicates and low-quality alignments (MQ<25). Final genome coverage was estimated using paleomix coverage and ignoring read groups, and the sex of each individual was assessed from the ratio of high-quality alignments against the autosomes and the X chromosome, expecting ~2:1 and ~1:1 ratios in males and females, respectively (table S1).

BAM alignment files were directly processed for estimating sequencing error rates, following the methodology from *(25,54)* leveraging three-days alignment between the ancient genome considered, a high-quality 'perfect' genome from a modern Arabian individual (ERR3465836), and an ancestral genome. Errors were estimated relative to the branch length leading to the 'perfect' genome, and broken down by substitution class (table S1 and fig. S4). BAM alignment files were also analyzed using PMDtools v0.60 *(67)* and mapDamage v2.2.1 (*68*), to assess the presence of signatures of post-mortem DNA damage. The sequence data generated from single-stranded DNA libraries prepared on extracts not treated with the USER enzymatic mix showed expected C→T nucleotide mis-incorporation patterns (*69),* increasing both towards template starts and ends (fig. S2AB). Similarly, the sequence data generated for the remaining samples (*i.e.* double-stranded DNA libraries prepared on extracts treated with the USER enzymatic mix) showed inflated C→T nucleotide mis-incorporation rates towards template starts, and symmetric profiles for their complementary G→A mis-incorporations towards template ends (fig. S2CD). The latter signatures were, however, only observed when conditioning analyses to CpG dinucleotides, in line with USER treatment eliminating C residues that have been degraded into Uracil residues, following post-mortem deamination (*70).* Moreover, we checked base compositional profiles using mapDamage v2.2.1 (*68*) as a further

assessment of the presence of post-mortem DNA damage signatures. The sequence data generated from single-stranded DNA libraries prepared on extracts not treated with the USER enzymatic mix showed the expected excess of purines at the positions located right upstream and downstream of sequence alignments in the reference genome (fig. S3), in line with depurination driving DNA fragmentation after death (*71*). The sequence data generated for the remaining samples, whose DNA extracts were USER treated, showed the expected excess of Cytosine residues at the positions located right upstream of sequence alignments in the reference genome. This was mirrored by an inflation of complementary Guanine residues at the positions located right downstream of sequence alignments in the reference genome. Combined, these signatures authenticate the sequence data generated as deriving from genuine ancient DNA molecules.

BAM alignment files were further processed to identify transversion SNPs, using the methodology from *(25,54).* Read ends were, however, not trimmed and the quality of sites potentially associated with post-mortem DNA damage were not masked, as the vast majority of the sequence data (99.88% of all aligned '*Collapsed'* or '*Collapsed truncated*' reads, and 99.76% of all aligned '*Paired'* reads) were produced following USER-treatment a treatment aimed at limiting the impact of post-mortem DNA damage. Briefly, the procedure used ANGSD (htslib: 1.16, build Dec 10 2022 14:56:47; *(72))* to retrieve counts of each nucleotide at those transversion positions that are covered in at least 80% of the specimens and are likely polymorphic in the overall genome sequence panel considered (-SNP_pval 1e-16 -remove_bads 1 -minMapQ 25 -minQ 30 -rmTrans 1 -rmTriallelic 1e-4 -C 50). Counts were further processed to randomly sample one nucleotide per position in every single sample, disregarding positions within the 99.5 quantile of the coverage distribution. This procedure returned a final TPED matrix including 9,386,235 pseudo-haploid positions in 227 specimens, consisting of the 67 genomes newly characterized in this study, and a subset of genomes previously sequenced and chosen to encapsulate the entire range of the lineages identified (table S1).

Phylogenetic reconstructions and population graph modelling

Mitochondrial read alignments were generated through the Paleomix procedure described above against the horse reference mitochondrial genome (Accession nb. NC_001640; *(73)).* The first 30 reference positions were copied at the end of the sequence to allow identification of reads mapping to both ends of a linearized circular genome, following *(59).* BAM files were processed one at a time with BCFtools (v1.8-31-g9ba4024, using htslib 1.7-41-g816a220; *(74)*) to call genotypes at sites with coverage of at least 5, and FMT/GQ ratios greater than or equal to 30. Genotypes were called considering the data diploid to account for the typically elevated heteroplasmic levels found in horses, including in clones *(75),* and DNA sequencing errors typical of ancient DNA data (*(69)*; table S1*).* Genotype variation was converted into FASTA files using paleomix vcf_to_fasta (v1.3.7; *(63)*), and mitochondrial haplotypes were aligned manually against the donkey mitochondrial reference haplotype (Accession nb. CM027722.2; *(76)),* which served as outgroup. Sites showing over 50% missingness as well as repeats located between positions 16,121-16,360 of the horse mitochondrial reference genome were disregarded, and the consensus of the first and last 30 nucleotide positions was rewritten to the first 30 positions, before excluding the last 30. We then added to this alignment the mitogenome sequences of one *E. przewalski* (MW348986.1) and eight *E. dalianensis* (MW348985.1, MW348987.1- MW348993.1) ancient specimens, published by Yuan et al. *(27),* to construct a Maximum Likelihood phylogeny in IQtree (v1.6.12; *(77)*). We carried out 1,000 bootstrap pseudo-replicates and ultrafast bootstrap approximation for assessing node support, and

considered the best substitution model according to the Akaike Information Criterion (AIC; GTR+F+R10) (Fig. 1C and fig. S5).

High-quality read alignments against the Y chromosome were processed according to the procedure used for detecting autosomal variation, excepting that: (1) analysis was restricted to the single copy regions identified by Felkel et al. *(62)*; (2) the -SNP_pval was increased to 1e-6, and; (3) positions covered in at least 50% of the male specimens were considered. This procedure returned a final TPED matrix including 16,142 haploid positions across the single copy Y chromosomal contigs from 130 specimens. Y chromosome phylogenies were carried out, following the same methodology used for mitochondrial analyses, tolerating up to 90% missing data per sample and resulting in a subset of 127 sequences (N=14,699 bp; fig. S6).

Phylogenetic affinities for autosomal transversion SNP variation were reconstructed using FastMe (v2.1.6.2; *(78))*, and assessing node support from 100 bootstrap pseudo-replicates using newick utils (v1.6; *(79)*; Fig. 3A). All phylogenies were plotted using R, and the ape, ggrepel, ggtree, tidytree and treeio libraries.

Phylogenetic trees incorporating admixture events were reconstructed using AdmixtureBayes *(32)* and OrientAGraph *(33)*, as two optimal methods for inferring optimal population graphs. These analyses used predefined population groups consisting of donkeys as outgroups, plus eight horse lineages, including A-EBer, A-IFC, A-LO48, E-NESib, E-NESib*, E-SERus, and URAL, while merging A-NBer and A-WBer, due to their close genetic affinities, to save computational running times (Fig. 3A). For both analyses, individual allele frequencies were stratified per site and per group using Plink v1.9 *(80)* (--freq –within), disregarding sites with no sequence data at the group level were disregarded (--mac 1), which left a total of 2,335,557 sites for the analyses. AdmixtureBayes *(32)* was run for a total of 200 million iterations (--n 40000000), and considering 20 MCMC chains and 10 admixture events at most (--max_admixes 10). The posterior distribution of admixture graphs was generated pruning the first 50% as burnin, and thinning one every 2,500 of the remaining (resulting in a final set of 1,000 trees). Convergence was checked using Gelman-Rubin convergence diagnostic across three independent analyses, showing posterior values tending to 1.0. Fig. 4A shows the population graph with the highest log-posterior in the posterior distribution, which represents 22.6% of the posterior graph space. The consensus graph across the graph posterior distribution and all graphs accounting each for at least 5% of the graph posterior distribution are also provided in fig. S15. OrientAGraph *(33)* analyses were run following Librado et al. *(54)*, running the maximum likelihood network orientation subroutine as part of search heuristic (-mlno), and considering up to 5 migration edges (-m) and blocks of 100 SNPs for estimating the covariance matrix. The model assuming M=5 migration edges was considered the most optimal (Fig. 4B), as: (1) it explained 99.9999867% of the genetic variance, and; (2) model residuals were lower than 2.1 times the average standard error observed between all population pairs. All models reconstructed assuming M=0 to M=5 are displayed on fig. S16, together with their respective residual fits from the Maximum Likelihood tree.

Population structure

Pairwise estimates of genetic proximity between samples were calculated as f3-outgroup statistics *(30)*, using 5 Mb genomic blocks for jacknifing in Calc-f3 *(31)* and the two donkey as outgroups, while masking sample pairs with less than 25,000 positions covered (fig. S10). Principal Component Analyses (PCA) were repeated in smartPCA *(81)*, turning on the AUTOSHRINK mode and activating the ‘inbreed’ option to account for pseudo-haploid data

(Fig. 2A and fig. S7-S9). Outgroups were removed from the matrix of autosomal variation as well as sites under linkage disequilibrium using Plink v1.9 *(80);* --indep-pairwise 500 10 0.2). Only variants represented at a minimal allele frequency of 5% were considered (--maf 0.05), resulting in a total of 2,133,241 sites. Samples JK162 (IMNH 1136/11898), JK273 (KU42626), JK274 (KU43413), JK275 (KU47538), JK278(KU47519), PH042 (P95.1.42), AV073 (Eq-Suh/2) and AV075 (Eq-Suh/5) were projected against the PCA space defined by the other samples using LSQ projection, to account for their relatively limited sequence coverage (average depth-of-coverage=0.01-0.41-fold) (Fig. 2A and fig. S7-S9).

The SNP matrix considered for PCA was also processed in ADMIXTURE (v1.3.0; *(29)*) to profile the proportions of main genetic ancestries in each individual sample (Fig. 3B and fig. S12). A range of K=2 to 10 genetic ancestries were considered, with K=4 cross-validated as the best option (--cv=10). Confidence intervals for genetic ancestry proportions were estimated from 100 bootstrap pseudo-replicates, setting the minor convergence criterion (-c) to 0.0001, for K=2 to K=4. Ancestry profiles were further evaluated using the Struct-f4 package *(31)* for the same range of genetic components (K=2 to K=10), and considering the full matrix of transversion SNPs, *i.e.* including donkey outgroups. The combination of the 5,619,600 possible non-redundant f4-statistics were first calculated using Calc-f4 *(31)*, forcing the two donkeys as a single outgroup, and jack-knifing through 5 Mb blocks. Individual ancestry proportions were then estimated using f4-statistics as input and running the Struct-f4.r function *(31)* for 20 million iterations for the first MCMC chain (assuming no admixture), and 100 million iterations for the second MCMC chain (assuming admixture between K ancestry components). Genetic ancestry profiles were plotted in R using the ggplot2 library, ordering samples according to their autosomal NJ tree genetic affinities (Fig. 3A, Fig. 3C, and fig. S13).

D-statistics of the form (Outgroup, X; URAL, Y), where X represent any of the A-EBer, A-IFC or A-LO48 population groups, and Y any of the E-NESib, E-NESib*, E-SERus and Rus45 individuals, were calculated using qpDstats v751 (*30*) and the whole matrix of SNP transversions (fig. S14A). Additionally, D-statistics of the form (Outgroup, X; Taymir, Y) were calculated using the same methodology (fig. S14B); here, we grouped together Late Pleistocene E-NESib individuals excavated in the Taymir peninsula, to represent the location in our data set that is located at the westernmost range of West Beringia, hence, least likely to have received some genetic influence from American horses). F4-ratios were calculated using qpF4RATIO (*30*) on the same data, considering genomic blocks of 5 Mb for jacknifing, and configurations of the form (((A,B),C),O). The tested samples tentatively shared genetic contributions from the B and C lineages. Here, A was assumed to be either A-LO48 or A-IFC; B comprised all members of the A-EBer lineage, and C included either a subset of E-NESib specimens showing no D-statistics evidence of possible admixture with A-EBer, A-IFC and A-LO48 populations (*i.e.* PH153, UP362, UP354 and Rus30x31; E-NESib$), or a subset of E-NESib specimens from the Taymir peninsula, located in the northwesternmost range of northeast Siberia, *i.e.* the farthest away from Beringia in the region. The estimated genetic contributions from the A-EBer lineage in the individuals tested are shown in Fig. 3D, when their confidence range was greater than zero.

Demographic trajectories

The past demographic trajectory of A-IFC horses, all radiocarbon dated to ~13 kyr B.P. (table S1), was reconstructed using GONE (v1.0, *(34)*) (Fig. 5A). Default parameters were used, except for the number of bootstrap pseudo-replicates considered, which was set to N=100, and the

PHASE option, which was turned to 0 to account for data pseudo-haploidization. Genetic distances were linearly interpolated from physical distances using the closest markers identified in the recombination map from Beeson et al. *(82)*. Following Librado et al. *(25)*, transversion SNPs along chromosomes 7, 11, 12 and 20 were removed to avoid local mis-assembly issues and unaccounted large-scale structural variation potentially affecting the validity of the recombination map. Only sites covered in at least 50% of the samples were considered, representing a total of 1,962,038 transversion positions. Time (*i.e.* number of generations prior to 13,088 kyr B.P., as the average radiocarbon dates of the A-IFC individuals) was converted in calibrated years B.P., assuming a generation time of 7.4 years, following the estimate recently published by Librado et al. *(25)*, as the average generation time across DOM2 and pre-DOM2 lineages from Eurasia in the last 15,000 years.

Radiocarbon dating and isotope measurements

The newly analyzed data include 24 specimens from North America, and 13 from Eurasia (tables S1 and S2). Collagen was isolated from fossil horse bones following standard protocols *(83)*. Radiocarbon dating and $\delta^{13}C$ and $\delta^{15}N$ isotope profiling was performed at the Keck AMS laboratory, University of California Irvine (USA). Samples of cortical bone were cleaned mechanically and aliquots of ~200mg were crushed to mm-sized chips. If contaminating conservation materials were present, samples were sonicated in acetone, methanol and ultrapure MQ water in a water bath cooled to well below the melting point of collagen. Bone was decalcified overnight at room temperature, using a measured amount of 1N HCl just sufficient to dissolve all of the bone mineral, if no collagen was present. The demineralized samples were washed with MQ water and gelatinized overnight at 60°C and pH=2, ultrafiltered in precleaned Vivaspin 15 devices to select the >30kDa molecular weight fraction, and freeze dried overnight. Aliquots of 2 mg of collagen were combusted under vacuum in quartz at 900°C with CuO and silver wire, and the resulting CO_2 was cryogenically purified and graphitized on Fe by hydrogen reduction for ^{14}C measurement by AMS on an NEC 0.5MV. 0.7 mg collagen aliquots were sealed in tin capsules and flash combusted in a Fisons NA1500NC elemental analyzer interfaced to a Finnigan Delta Plus isotope ratio mass spectrometer for elemental analyses and $\delta^{13}C$ and $\delta^{15}N$ measurements.

Isotope database compilation

The dataset used in our study is a compilation of 3,809 published (N=3,585) and newly generated (N=224) data, including calibrated radiocarbon dates (N=3,063), $\delta^{15}N$ (N=3,762), and $\delta^{13}C$ (N=3,053) values from collagen, from a total of 115 individual studies spanning Europe, Asia, and North America, with a great majority of late Pleistocene (>11,700 years) individuals. The compiled published data include mostly obligate grazers with 292 bison, 996 horses, 504 mammoths, 31 sheep, 316 wooly rhinoceros and 35 aurochs. The remaining specimens are browsers and mixed browsers/grazers, including 563 reindeer, 427 deer, 211 muskox, 122 bears, 119 saiga antelopes, 108 mastodons, 36 moose, four chamois, five ibex, four camels, five sloths, plus three ground squirrels, four grouse, and seven rabbits. A few omnivores and carnivores are also considered, including seven wolves, one fox and one cave lion. The database also includes approximate latitude and longitude data for each individual sample. In the majority of cases, geographic coordinates were reported by the authors in the publication. When not originally reported, Google Earth was used to georeference the reported geographic information (*i.e.* maps and site locality). When necessary, authors of publications were contacted to clarify locality

information. The method of georeferencing and its associated uncertainty are reported in the database, which is available in table S2 (along with the full citations of the original sources from which the data sets were derived). The data can be filtered by museum, museum ID, species and taxon, region, diet, sample type or analytical substrate.

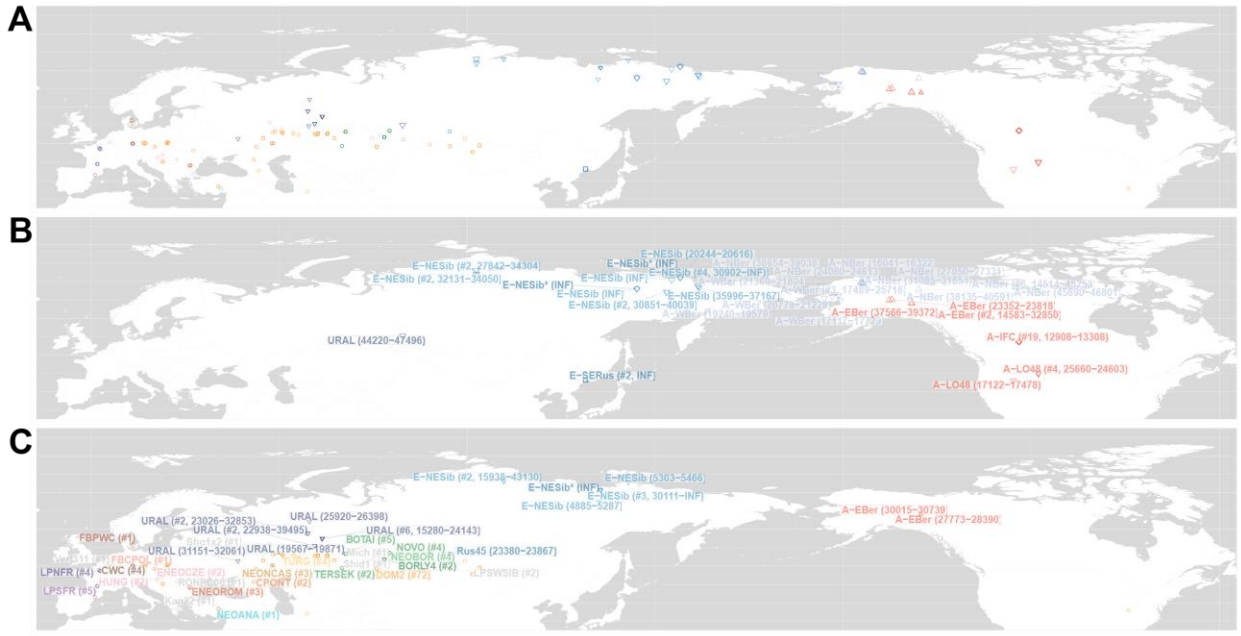

Fig. S1. Geographic distribution of the samples investigated in this study. (A) Summary map of all specimens, including those previously and newly sequenced. Shapes and colors are consistent with those used in the various figures, and reflect the different population groups, in line with those from previous publications *(25)*. (B) Summary map of the specimens newly sequenced in this study. Sample labels include first a name, followed by a three-letters code referring to their country of origins, and the midpoint of the radiocarbon date in calibrated years B.P. (INF is shown for specimens associated with infinite radiocarbon measurements). For clarity, a single annotation is indicated in locations where multiple specimens were analyzed. In such cases, labels indicate the number of specimens (#) and provide their radiocarbon range (see table S1 for individual information). (C) Same as (B), for the specimens previously sequenced and used as a comparative panel.

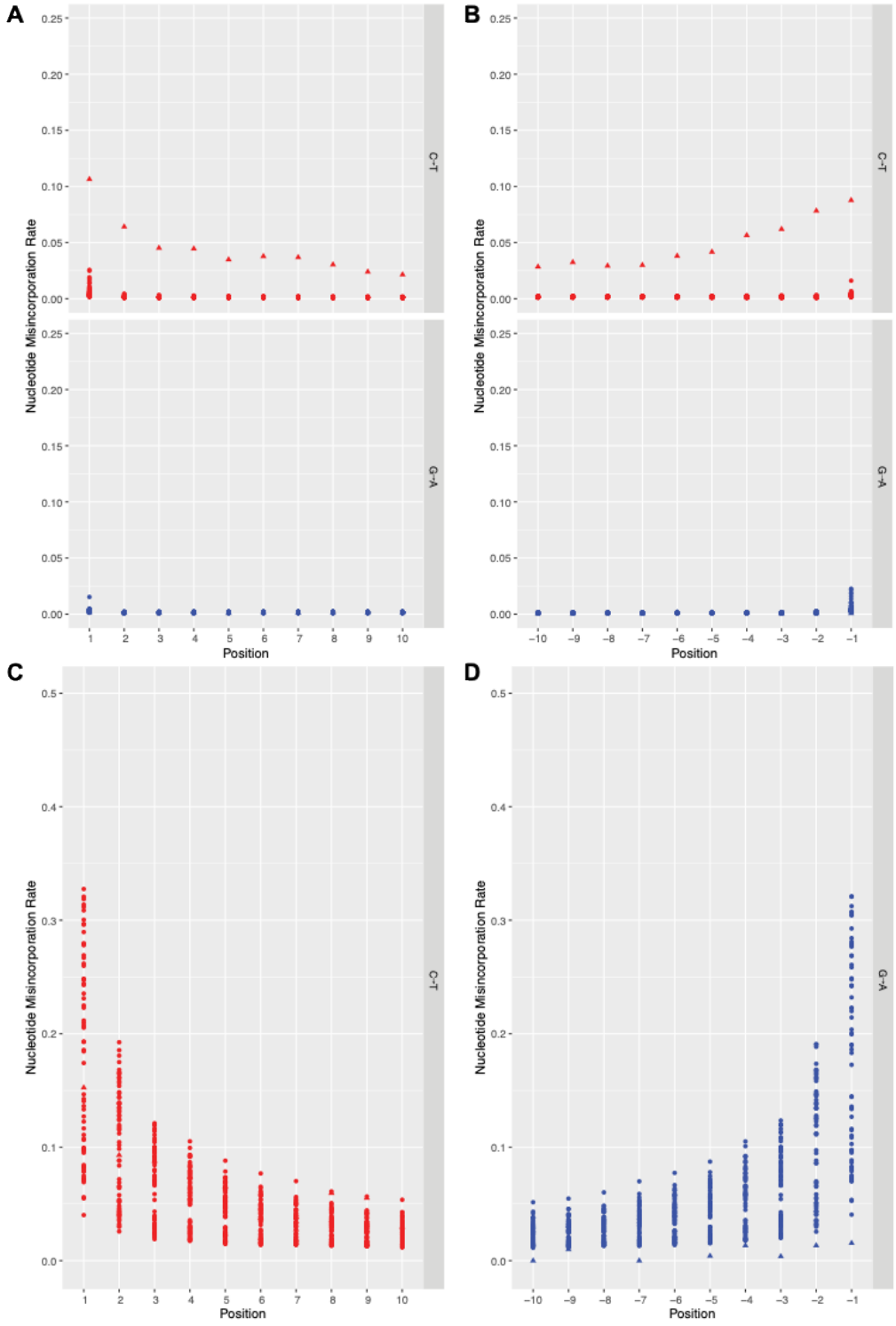

Fig. S2. Nucleotide mis-incorporation patterns typical of ancient DNA damage. (A) C→T (Top) and G→A (Bottom) nucleotide mis-incorporation rates at the first 10 positions of read

alignments. (B) Same as (A), but for the last 10 positions of read alignments. Sample JK162 is indicated with a filled triangle, while all the other samples are shown with filled circles. JK162 was prepared on raw DNA extracts (*i.e.* not treated with the USER enzymatic mix), and using the single-stranded DNA library preparation protocol from Kapp et al. *(57)*. As expected, it shows highly-inflated C→T mis-incorporation rates, relative to all other specimens for which the vast majority of the sequence data was generated on USER-treated DNA extracts, and following the double-stranded DNA library procedure from Librado et al. (*25,54*). The latter show the expected inflation of C→T nucleotide mis-incorporations at the first aligned nucleotide, and their complementary G→A at the last position of the alignment. In contrast, the profile of sample JK162 show an inflation towards both alignment starts and ends, but only of C→T nucleotide mis-incorporations, as expected when using single-stranded DNA libraries *(69)*. (C) C→T nucleotide mis-incorporation rates at the first 10 positions of read alignments, conditioning on CpG dinucleotide positions only. (D) G→A nucleotide mis-incorporation rates at the first 10 positions of read alignments, conditioning on CpG dinucleotide positions only. When subjected to post-mortem deamination, methylated CpG dinucleotides are modified into TpG dinucleotides, generating CpG→TpG mis-incorporations during sequencing *(70)*. Conditioning on CpG dinucleotides, thus, offers an opportunity to investigate the presence of nucleotide mis-incorporation related to post-mortem deamination of Cytosines, even if ancient DNA extracts were treated by the USER enzymatic mix. All samples show the expected inflation of C→T nucleotide mis-incorporation rates towards alignment starts (panel C). All samples, but JK162, also show the expected inflation of complementary G→A nucleotide mis-incorporation rates towards alignment ends (panel D). Sample JK162 is not expected to show inflated G→A nucleotide mis-incorporation towards alignment ends, due to the single-stranded DNA library preparation protocol that was used.

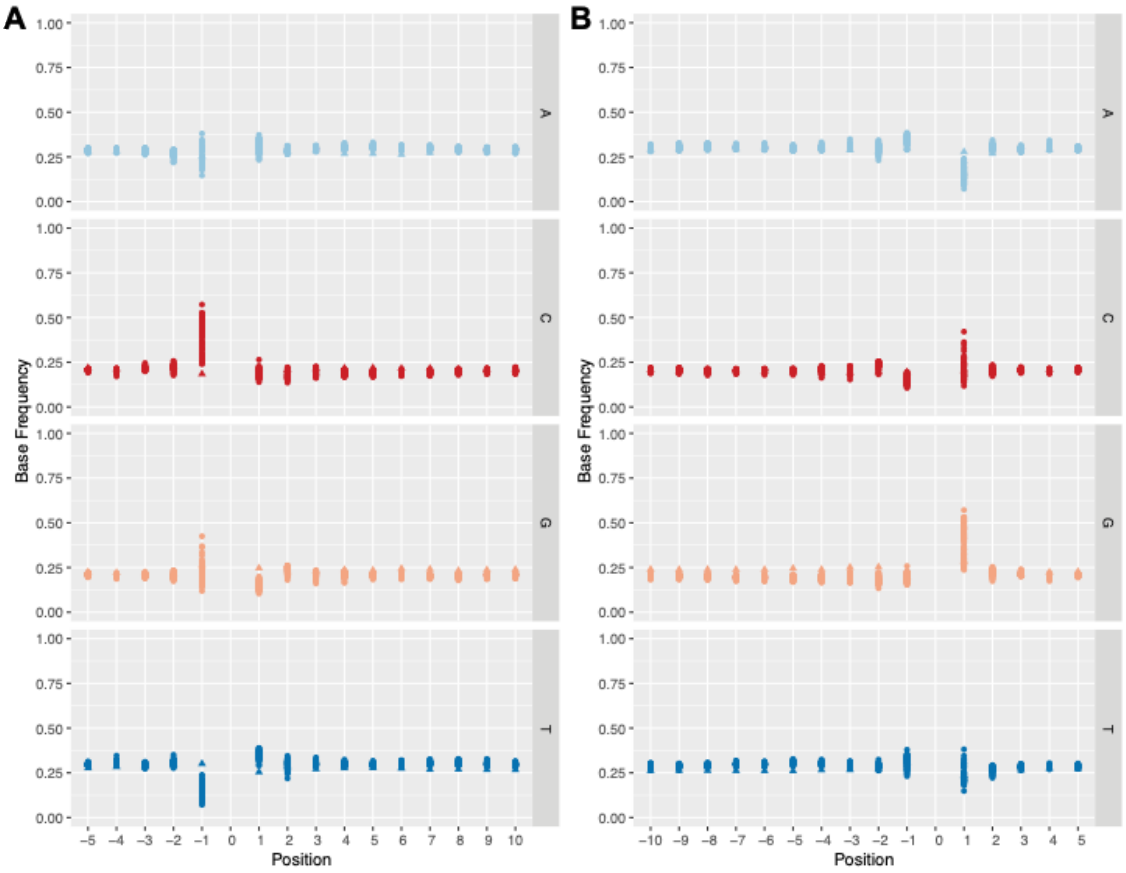

Fig. S3. Base composition profiles. (A) Base frequency for the first 10 alignment positions between reads and the reference genome (1 to 10), and the five reference positions preceding alignment starts (-5 to -1). (B) Base frequency for the last 10 alignment positions between reads and the reference genome (-10 to -1), and the five reference positions following alignment ends (1 to 5). Sample JK162 is indicated with a filled triangle, while all the other samples are shown with filled circles. JK162 was prepared on raw DNA extracts (*i.e.* not treated with the USER enzymatic mix), and using the single-stranded DNA library preparation protocol from Kapp et al. *(57)*. Due to depurination driving post-mortem DNA fragmentation (*71*), the base compositions of the first nucleotide positions preceding and following the alignments are slightly inflated in Guanine residues. All the other samples, for which the vast majority of the sequence data were generated following treatment of raw DNA extracts with the USER enzymatic mix, show an inflation of Cytosine residues. This aligns with USER cleaving DNA templates at those Cytosine positions that have been deaminated post-mortem (*69*). The base composition profiles of those specimens are also inflated in complementary Guanine residues at the positions immediately following read alignments, in line with the expectations of the double-stranded DNA library preparation protocol used *(69)*.

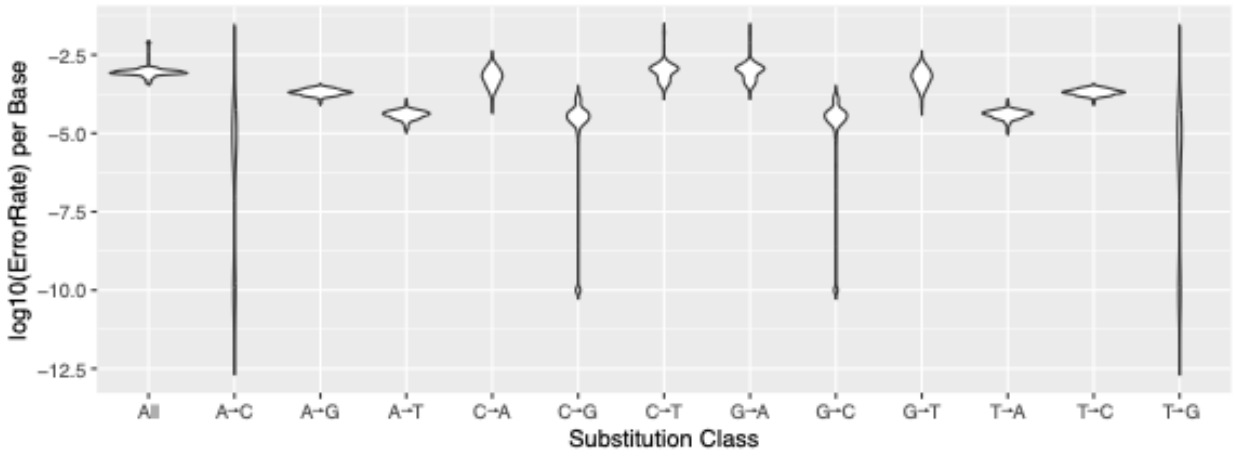

Fig. S4. Genome sequence error rates (per base). Individual error rates per base are provided in table S1. The figure displays the distribution of the overall ('All') error rates (*i.e.* combining all substitution classes), and those of individual substitution classes (A→C, A→G, A→T, C→A, C→G, C→T, G→A, G→C, G→T, T→A, T→C, and T→G). Error rates are $\log_{10}$ transformed for clarity. C→T and G→A transitions show inflated error rates than their reciprocal transitions (*i.e.* T→C and A→G), in line with the presence of nucleotide mis-incorporations at Cytosine sites that have been damaged by deamination post-mortem (*67-69,71*). The outlier sample showing an elevated overall error rate corresponds to specimen JK162 (IMNH 1136/11898), which is the least covered and for which only target enrichment data were generated.

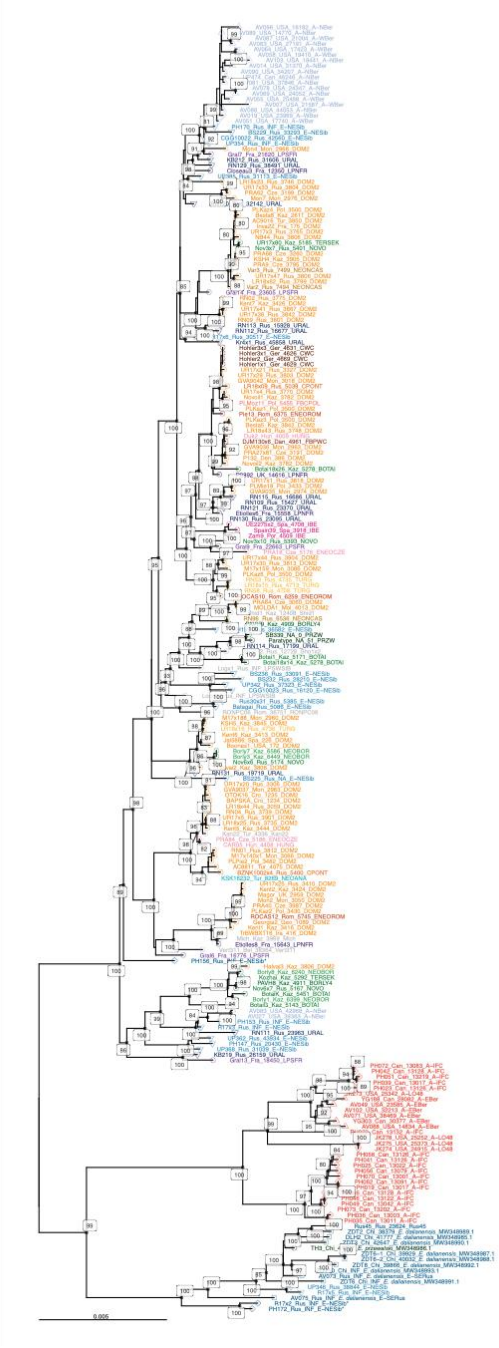

Fig. S5. Maximum Likelihood (ML) tree for mitochondrial DNA (N=16,420 bp).
Phylogenetic reconstruction was carried out using IQtree (v1.6.12; *(77)*) and the best substitution model identified according to the Akaike Information Criterion (AIC; GTR+F+R10 substitution model). The *E. przewalzki* and *E. dalianensis* sequences previously published by Yuan et al. *(27)* are indicated with reference to their Genbank accession numbers and added for comparison. Node supports (%) are displayed when greater than 80% as estimated from 1,000 replicates and ultrafast bootstrap approximation. Trees were manually rooted using donkeys as outgroups (not shown). A circularized version of this tree is shown as Fig. 1C.

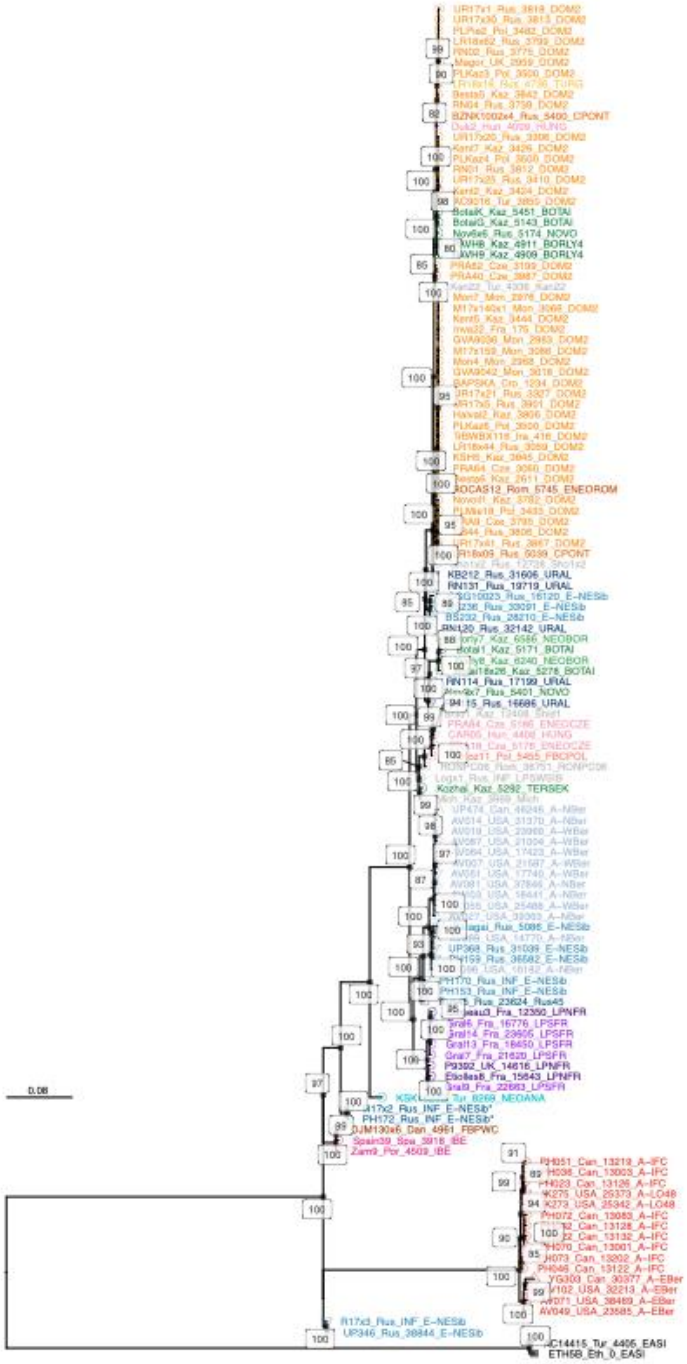

Fig. S6. Maximum Likelihood (ML) tree for Y-chromosomal DNA (N=14,699 bp). Phylogenetic reconstruction was carried out using IQtree (v1.6.12; *(77)*) and the best substitution model identified according to the Akaike Information Criterion (AIC; K3P+R4). Node supports (%) are displayed when greater than 80% as estimated from 1,000 replicates and ultrafast bootstrap approximation. Trees were manually rooted using donkeys as outgroups (not shown).

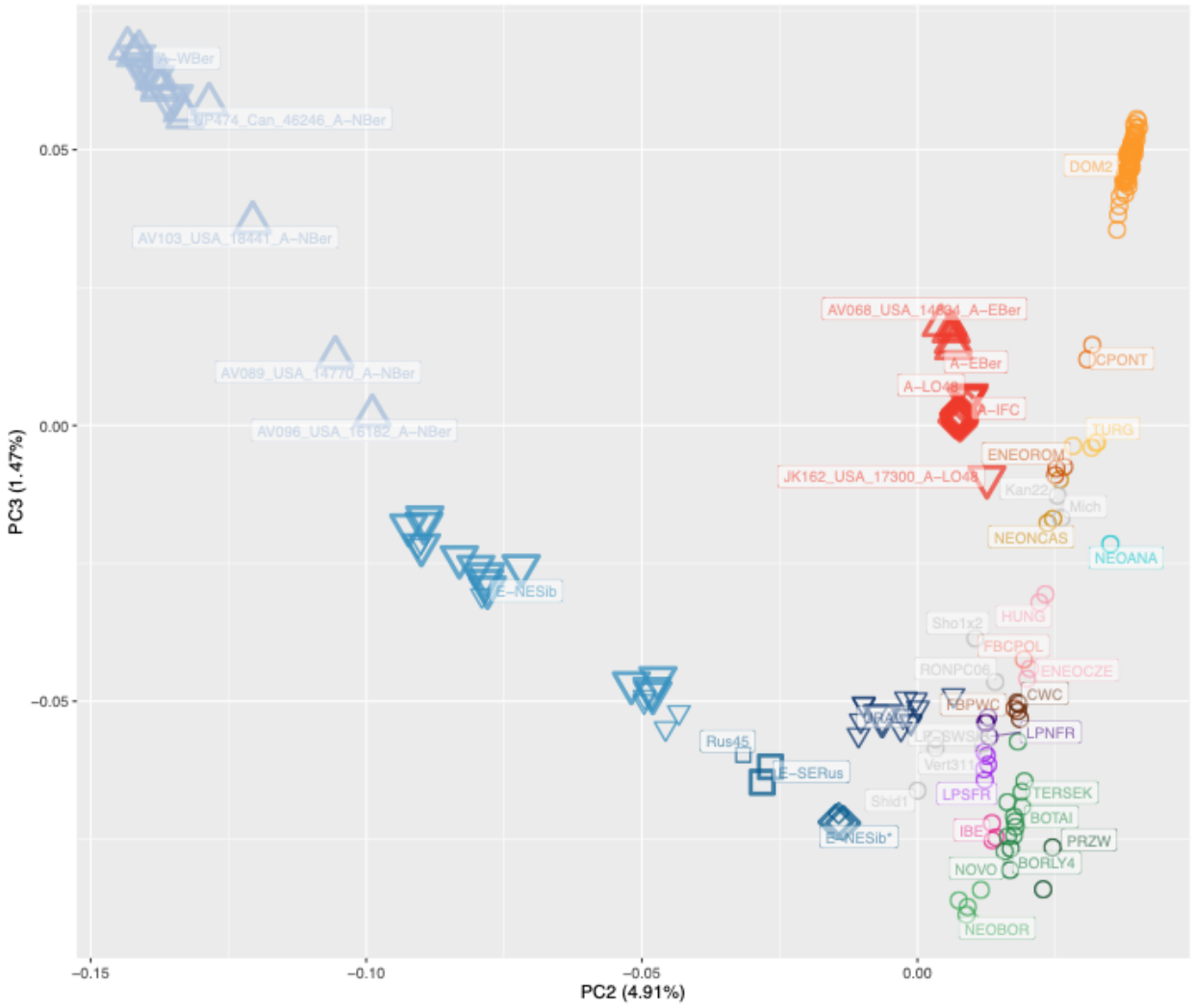

Fig. S7. Principal Component Analysis (PCA): PC2 versus PC3. The AUTOSHRINK mode was applied, and a total of eight samples were projected on the PC space defined by the remaining samples, due to coverage limitations (and the absence of shotgun sequence data for JK162). The eight samples projected are: JK162 (IMNH 1136/11898), JK273 (KU42626), JK274 (KU43413), JK275 (KU47538), JK278(KU47519), PH042 (P95.1.42), AV073 (Eq-Suh/2) and AV075 (Eq-Suh/5) (table S1). Labels indicate the main lineages, except for a few remarkable samples. Newly sequenced samples are highlighted with larger sizes. The proportion of the variance explained by the second and third PCs (PC2 and PC3) is shown between parentheses. The positions of the different samples along PC1 and PC2 are shown on Fig. 2A.

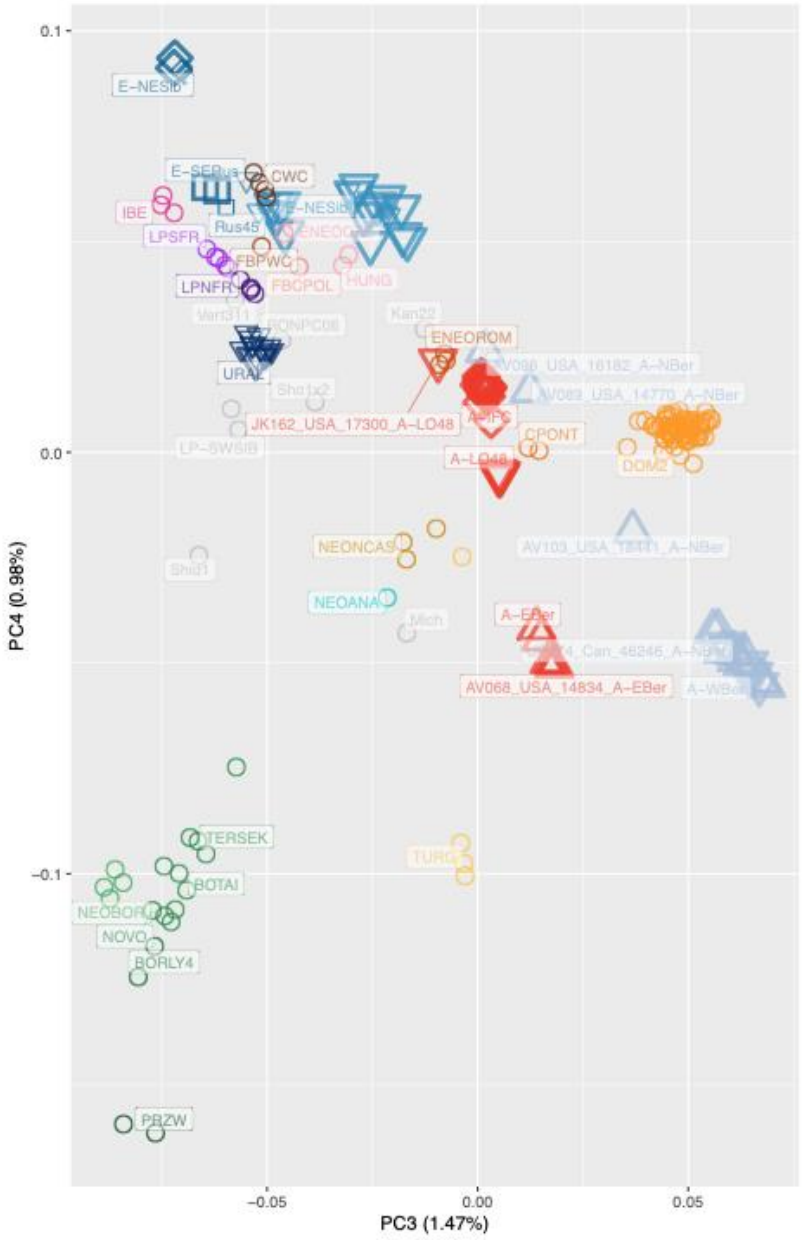

Fig. S8. Principal Component Analysis (PCA): PC3 versus PC4. The AUTOSHRINK mode was applied, and a total of eight samples were projected on the PC space defined by the remaining samples, due to coverage limitations (and the absence of shotgun sequence data for JK162). The eight samples projected are: JK162 (IMNH 1136/11898), JK273 (KU42626), JK274 (KU43413), JK275 (KU47538), JK278(KU47519), PH042 (P95.1.42), AV073 (Eq-Suh/2) and AV075 (Eq-Suh/5) (table S1). Labels indicate the main lineages, except for a few remarkable samples. Newly sequenced samples are highlighted with larger sizes. The proportion of the variance explained by the third and fourth PCs (PC3 and PC4) is shown between parentheses. The positions of the different samples along PC1 and PC2 are shown on Fig. 2A.

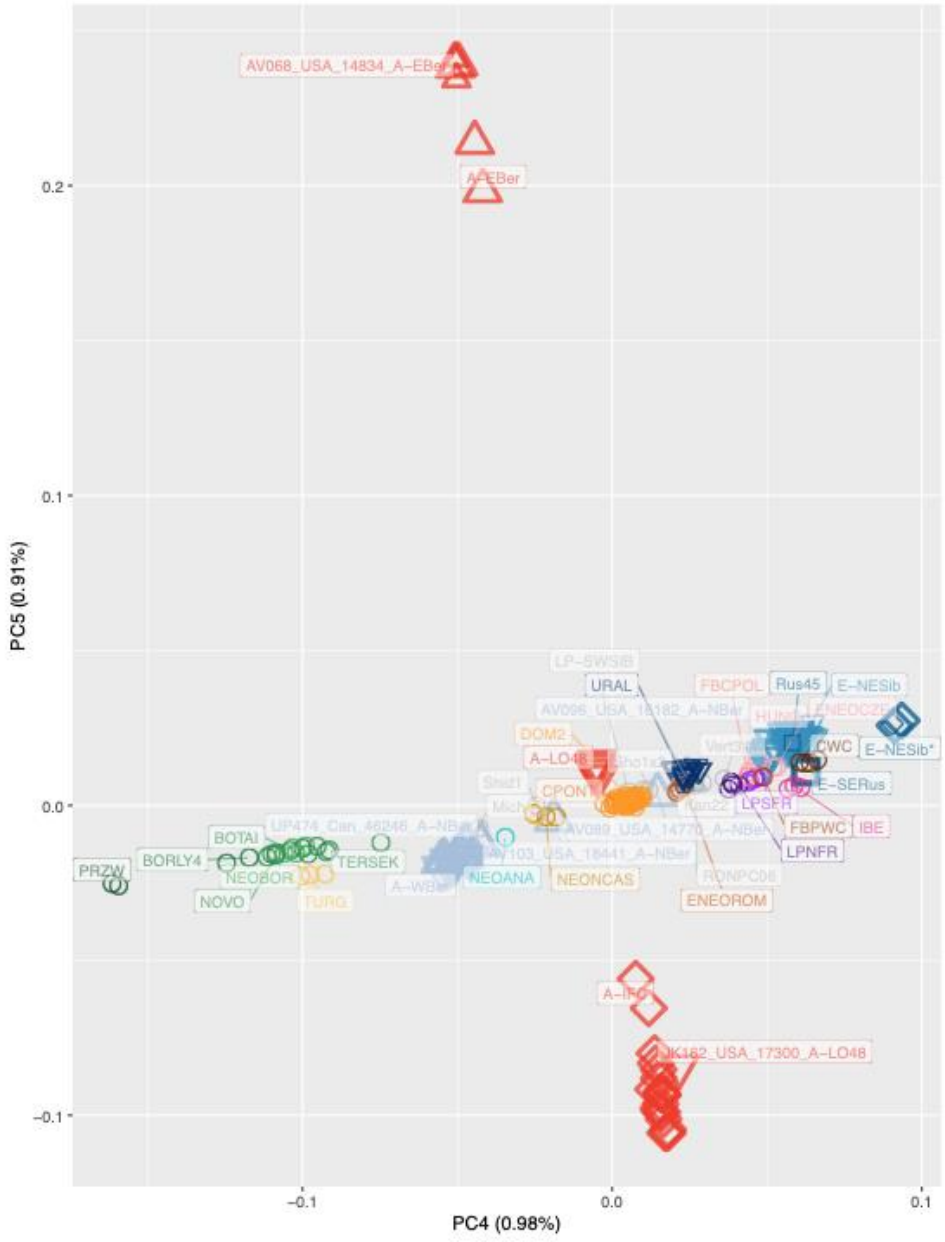

Fig. S9. Principal Component Analysis (PCA): PC4 versus PC5. The AUTOSHRINK mode was applied, and a total of eight samples were projected on the PC space defined by the remaining samples, due to coverage limitations (and the absence of shotgun sequence data for JK162). The eight samples projected are: JK162 (IMNH 1136/11898), JK273 (KU42626), JK274 (KU43413), JK275 (KU47538), JK278(KU47519), PH042 (P95.1.42), AV073 (Eq-Suh/2) and AV075 (Eq-Suh/5) (table S1). Labels indicate the main lineages, except for a few remarkable samples. Newly sequenced samples are highlighted with larger sizes. The proportion of the variance explained by the fourth and fifth PCs (PC4 and PC5) is shown between parentheses. The positions of the different samples along PC1 and PC2 are shown on Fig. 2A.

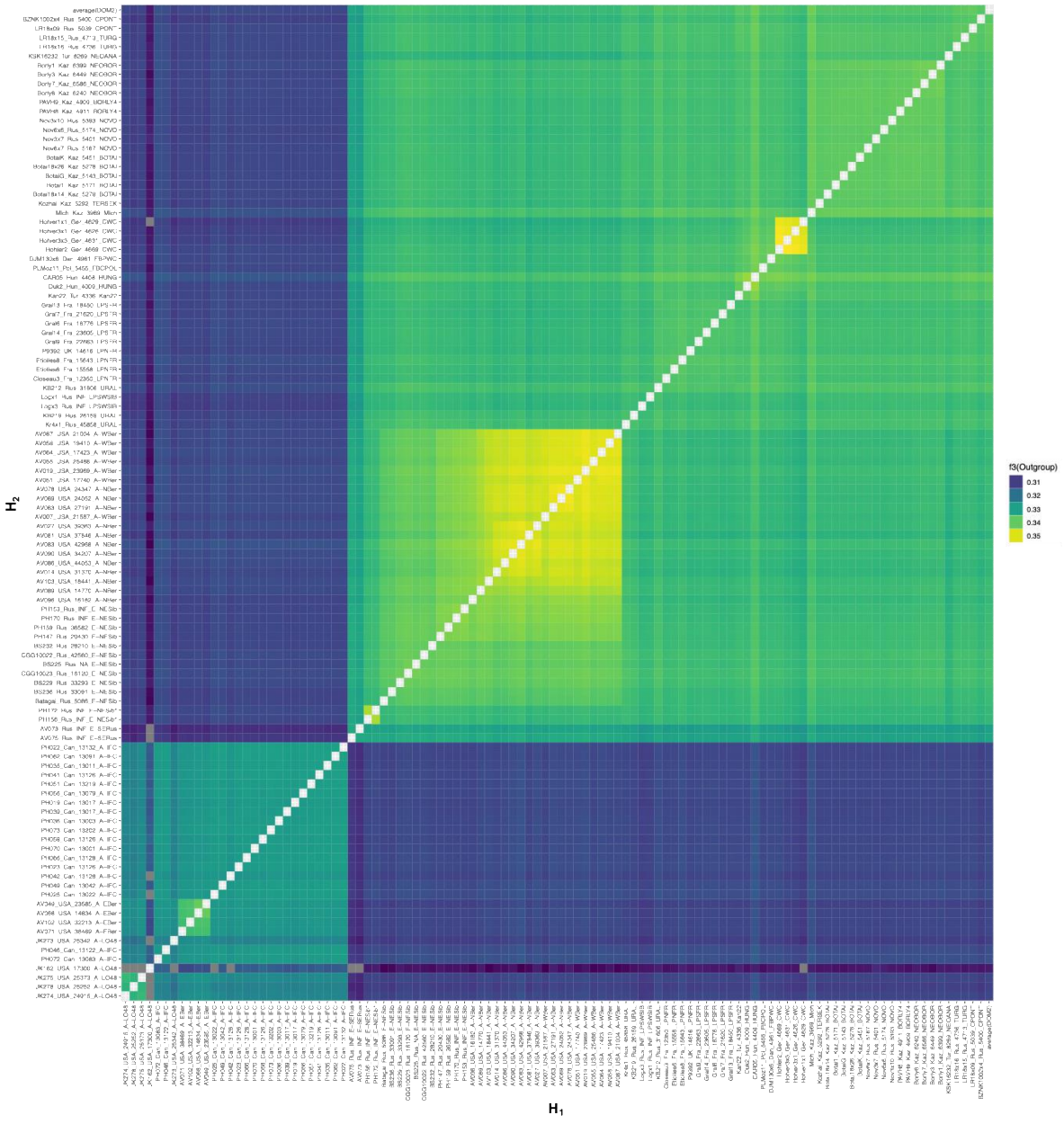

Fig. S10. f3-outgroup statistics. The two donkey genomes present in our genome panel were used as outgroups. Statistics are in the form: (H_1,H_2; Outgroup). Samples are ordered according to their phylogenetic placement in Fig. 3A. f3-outgroup statistics calculated from less than 25,000 sites are masked. The sequence data generated for sample JK162 were minimal (table S1), and only resulted from target-enrichment experiments, in contrast to all the remaining samples.

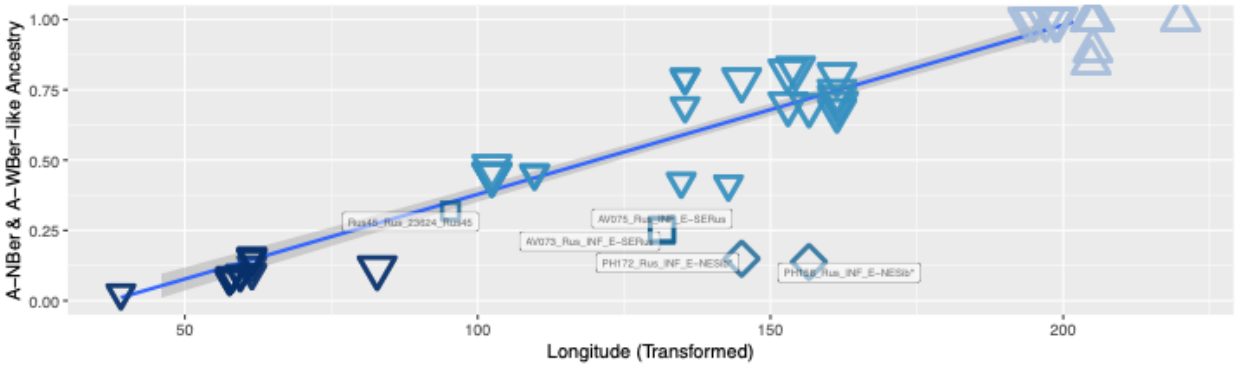

Fig. S11. Linear regression of the ADMIXTURE (*29*) genetic ancestry maximized in A-NBer and A-WBer genomes against longitude. The fitted Pearson linear regression model is shown with a blue line, with standard errors in grey. The labelled samples, including E-NESib*, E-SERus and Rus45 individuals, were not included in the model, as from different genetic backgrounds. Longitude was transformed by adding 360 degrees when inferior to -30, to place the American continent in continuity with Eurasia.

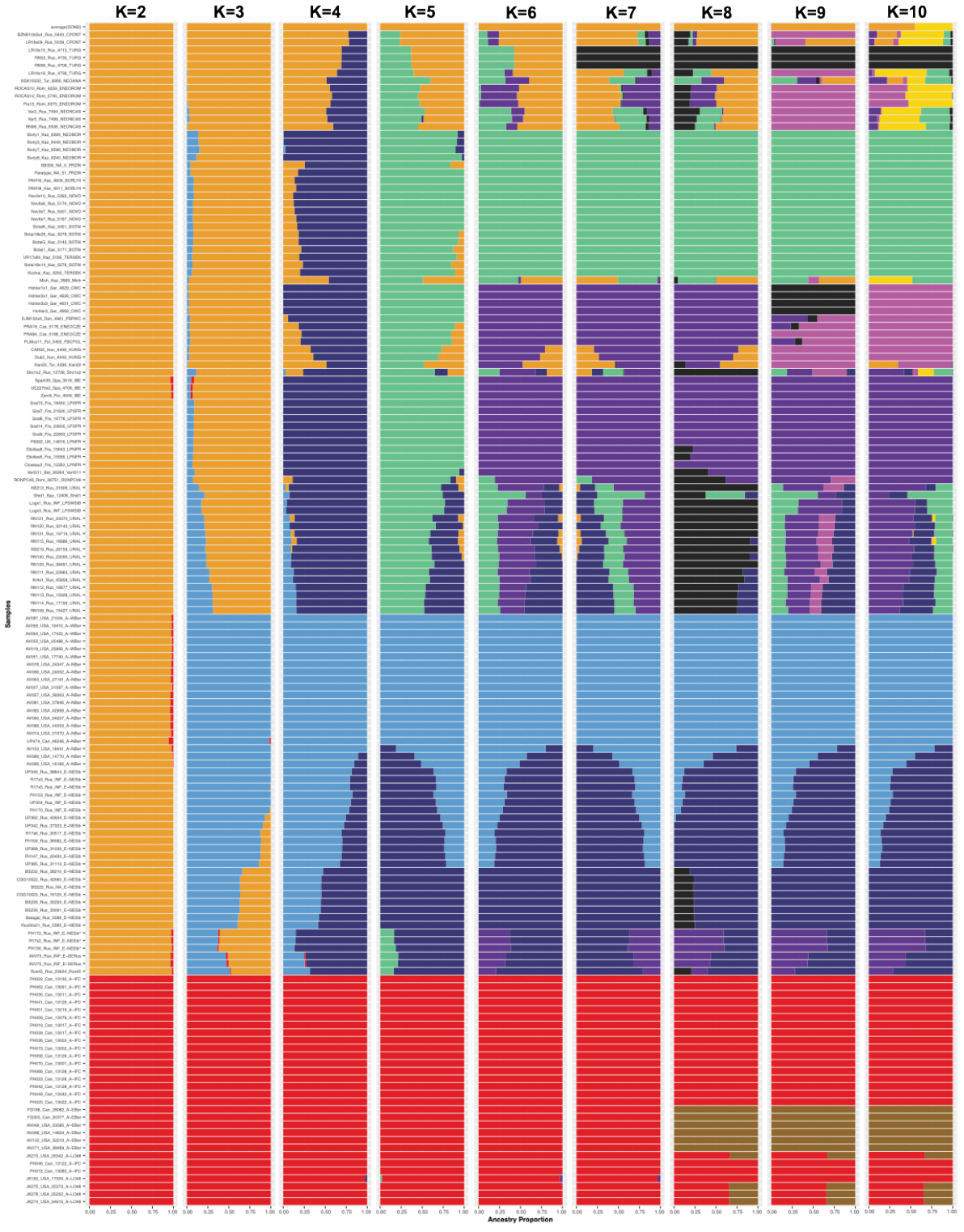

Fig. S12. ADMIXTURE (*29*) genetic ancestry profiles from K=2 to K=10. K=4 is shown on Fig. 3B, as the optimal number of genetic ancestries following cross-validation.

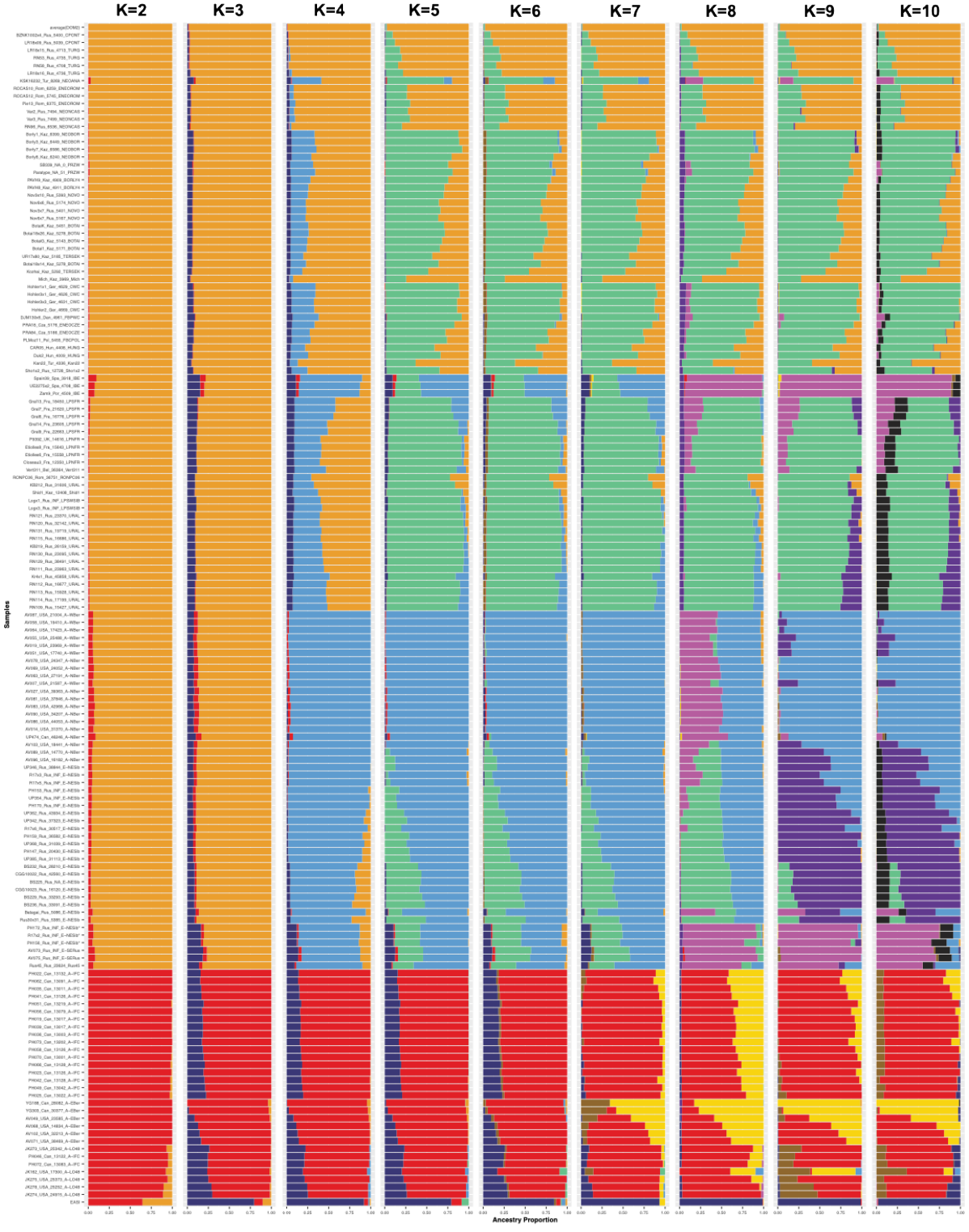

Fig. S13. Struct-f4 *(31)* ancestry profiles from K=2 to K=10. K=6 is also shown on Fig. 3C.

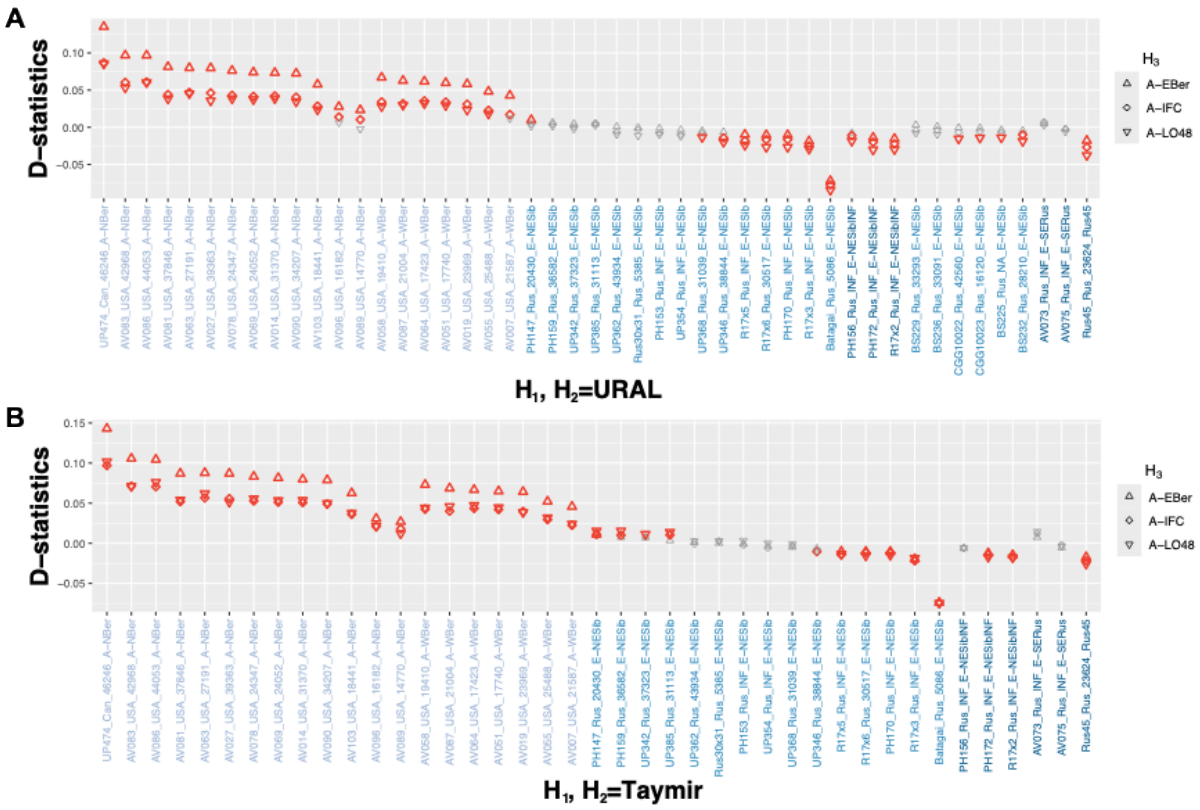

Fig. S14. D-statistics *(30)*. (A) D-statistics of the form (Donkeys, H_3; H_2, H_1), where H_1 represents the sample indicated on the x-axis, H_2 groups together members of the URAL lineage and H_3 comprises the members of either A-EBer, A-IFC or A-LO48 populations, were calculated using qpDstats. (B) Same as (A), excepting that H_2 groups together Late Pleistocene samples from the Taymir Peninsula (located in the westernmost range of West Beringia; *i.e.* BS229, BS225, BS232, BS236, CGG10022, and CGG10023; table S1). Positive (negative) D-statistics indicate an excess of genetic sharedness between H_1 (H_2) and H_3. D-statistics were sorted from greatest to lowest values in each of the population groups considered for H_1 individuals. Red colors reflect those statistically significant tests, correcting for multiple testing (Holm correction, *p*-value < 0.05).

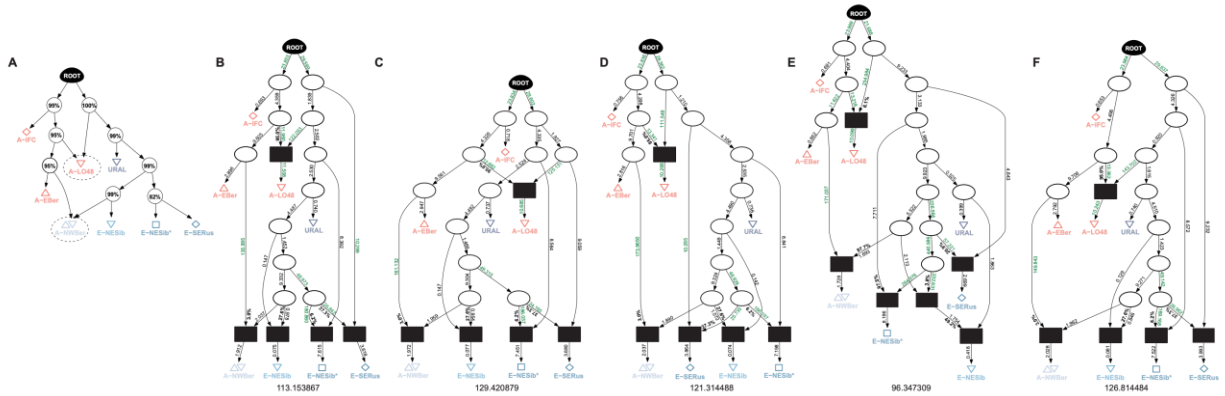

Fig. S15. AdmixtureBayes *(32)* population graphs. (A) Consensus population graph. Percentages reflect the posterior confidence received by each node. Population groups formed by admixture are surrounded with dashed circles. (B) Most common population graph in the graph posterior distribution (posterior probability=36.7%), with corresponding drift and admixture estimates. A simplified version of this graph is also represented in Fig. 4A, as the one showing the greatest posterior probability. (C) Second most represented population graph in the graph posterior distribution (22.6%), with corresponding drift and admixture estimates. A simplified version of this graph is also represented in Fig. 4B; it represents the one associated with the greatest log-posterior. (D) Same as (C), for the third most represented graph (14.8%). (E) Same as (C), for the fourth most represented graph (7.1%). (E) Same as (C), for the fifth most represented graph (5.7%). All other graphs together sampled represent less than 5% of the posterior distribution. Open circles and black squares indicate nodes and admixture events, respectively. Genetic drift and admixture proportions are indicated next to arrows with numbers (multiplied 100 times for clarity), and percentages, respectively. Branches showing substantial drift (≥0.1, *i.e.* 10.0 when multiplied 100 times) are colored in green. The respective log-posteriors are indicated below each model.

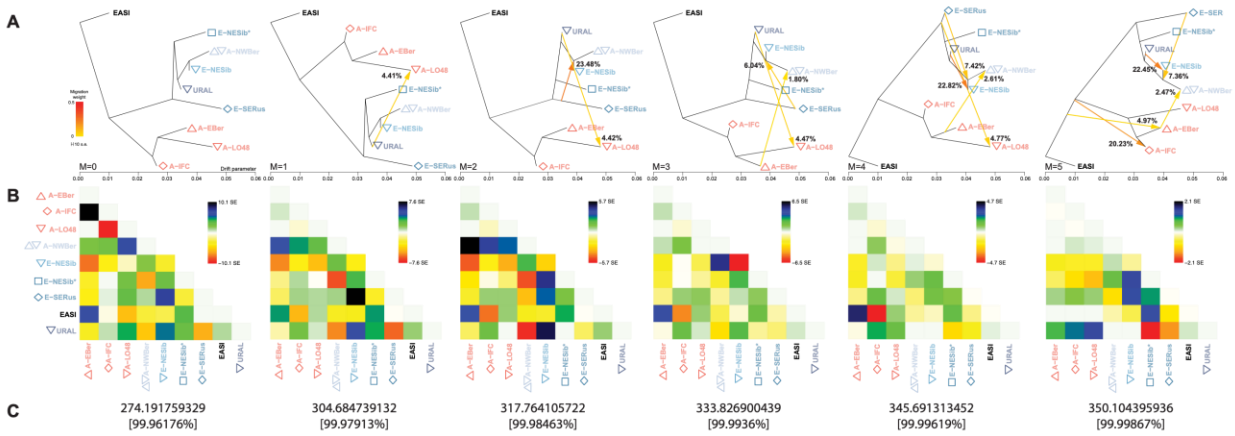

Fig. S16. OrientAGraph *(33)* population graphs, and residuals to fit. (A) Best population graphs assuming K=0 to K=5 migration edges. The proportions reported reflect the estimated admixture contribution resulting from a migration pulse from one source to one sink population. (B) Residuals to fit for the best population graphs obtained assuming K=0 to K=5 migration edges. (C) Model likelihood (top) and fraction of variance explained (bottom, between square brackets) for models including M=0 to M=5 migration edges.

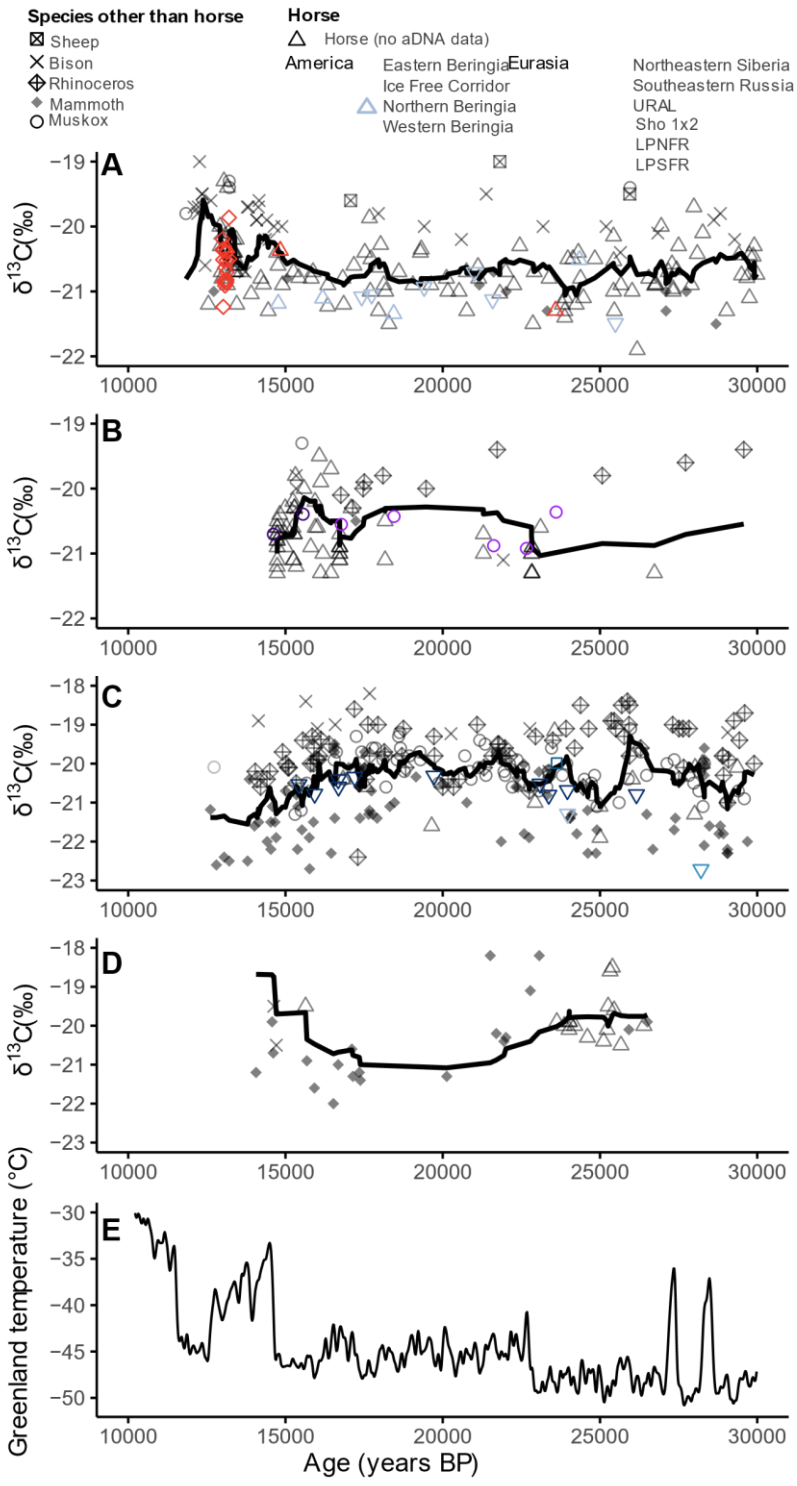

Fig. S17. Carbon isotopes. Time-series (years B.P.) of stable carbon isotope values in collagen of megafauna across different regions (table S2), including (A) Beringia; (B) Europe; (C) Siberia; (D) Continental North America, and; (E) temperature record in Greenland *(51)*. The curves represent the average of a 10 points sliding-window.

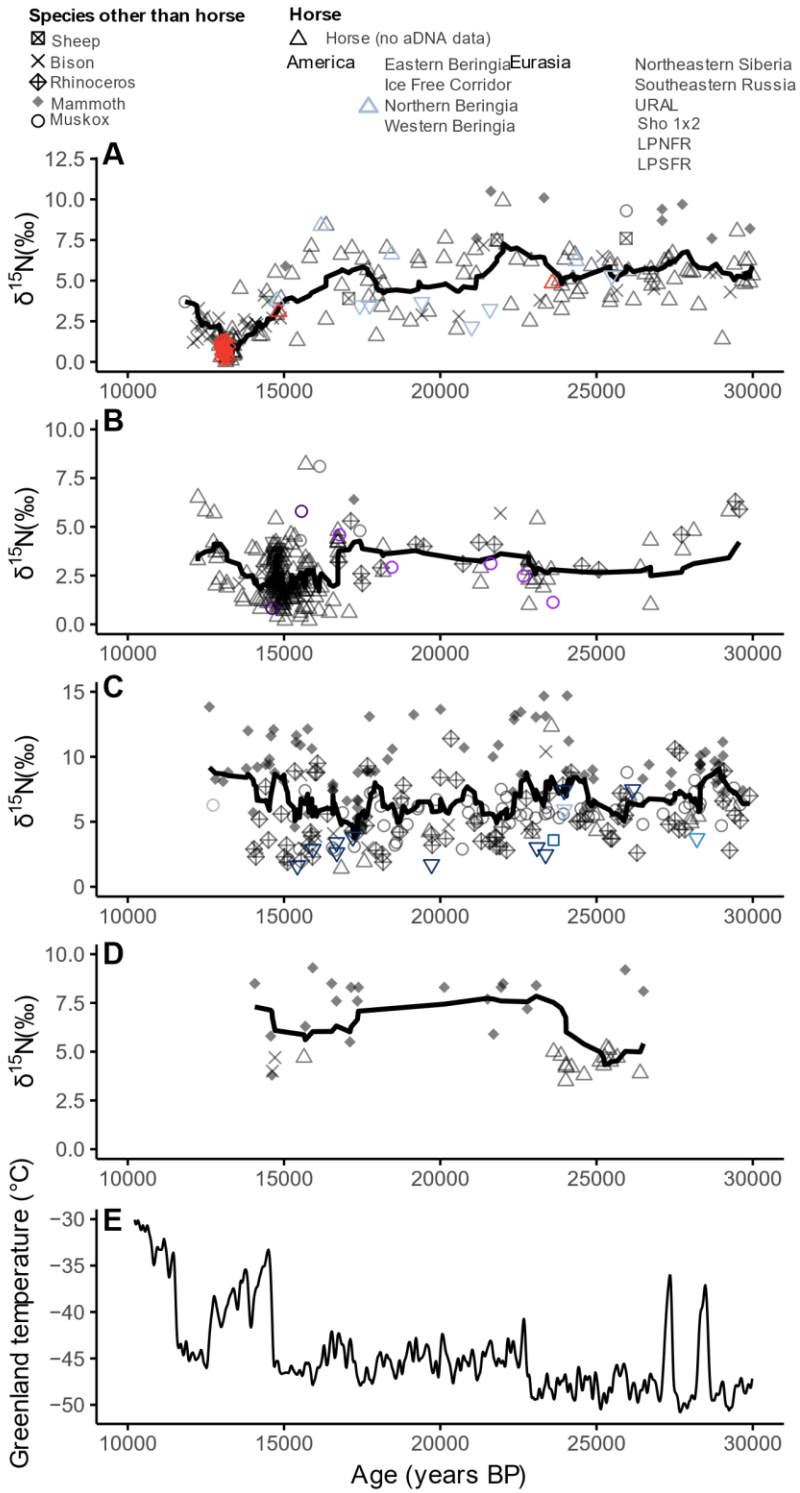

Fig. S18. Nitrogen isotopes. Time-series (years B.P.) of stable nitrogen isotope values in collagen of megafauna across different regions (table S2), including (A) Beringia; (B) Europe; (C) Siberia; (D) Continental North America, and; (E) temperature record in Greenland *(51).* The curves represent the average of a 10 points sliding-window.

Table S1. Sample information.

The table includes details (including locality information, stable isotope/C and N isotope data and radiocarbon dates) for all specimens (both previously published and those analyzed here for the first time). Labels refer to population groups showing genetic homogeneity, with reference to previous work. Sample names refer to a unique identifier, followed by a 3-letters country code and the age, either in calibrated years B.P. (Before Present) (or calendar years (B)CE ((Before) Common Era; the 'm' prefix indicating BCE, for consistency with previous publication). Information about the ancient DNA data generated at CAGT and UCSC is provided, including the number of independent DNA libraries constructed, respective sequencing efforts, final mitogenome and EquCab3 nuclear genome coverage, and estimated error rates. The biological sex of each specimen was inferred from the ratio of high-quality unique reads aligned on the X chromosome and the autosome, accounting for the chromosome size difference. The table then provides the results from a number of analyses presented in the main text, including ADMIXTURE *(29)* profiles (K=2 to K=4, with respective uncertainties in ancestry component estimates), F4 ratios *(30)* considering various conformations (((A,B),X,C),Outgroup), and Struct-f4 *(31)* profiles (K=2 to K=10).

Table S2. Carbon and nitrogen isotope compilation of late Pleistocene megafauna.

Compilation of radiocarbon dated samples with bone collagen carbon and nitrogen isotope data from the northern hemisphere. Metadata includes sample location (locality, region, latitude and longitude), detailed radiocarbon and isotope analysis metadata (*i.e.* collagen yield, $\delta^{13}C_{collagen}$, $\delta^{15}N_{collagen}$), and biological information (species, diet, analytical matrix). References for the compilation are given in the database and in the Supplementary Information.

References and Notes

1. M. Hunska Tašunke Icu, A. Luta Wiŋ, A. Nujipi, T. Omniya, M. Gonzalez, B. Means, S. High Crane, Mažasu, B. Dull Knife, W. Wiŋ, Y. Running Horse Collin, "Standing for *Unči Maka* (Grandmother Earth) and All Life: An Introduction to Lakota Traditional Sciences, Principles and Protocols and the Birth of a New Era of Scientific Collaboration" (Maxwell Museum Technical Series, no. 42, 2023).

2. W. A. Oquilluk, L. L. Bland, *People of Kauwerak: Legends of the Northern Eskimo* (AMU Press, 1973).

3. F. A. Smith, E. A. Elliott Smith, A. Villaseñor, C. P. Tomé, S. K. Lyons, S. D. Newsome, Late Pleistocene megafauna extinction leads to missing pieces of ecological space in a North American mammal community. *Proc. Natl. Acad. Sci. U.S.A.* **119**, e2115015119 (2022). doi:10.1073/pnas.2115015119 Medline

4. Y. Malhi, C. E. Doughty, M. Galetti, F. A. Smith, J.-C. Svenning, J. W. Terborgh, Megafauna and ecosystem function from the Pleistocene to the Anthropocene. *Proc. Natl. Acad. Sci. U.S.A.* **113**, 838–846 (2016). doi:10.1073/pnas.1502540113 Medline

5. E. J. Lundgren, J. Bergman, J. Trepel, E. le Roux, S. Monsarrat, J. A. Kristensen, R. Ø. Pedersen, P. Pereyra, M. Tietje, J.-C. Svenning, Functional traits-not nativeness-shape the effects of large mammalian herbivores on plant communities. *Science* **383**, 531–537 (2024). doi:10.1126/science.adh2616 Medline

6. P. Jaureguiberry, N. Titeux, M. Wiemers, D. E. Bowler, L. Coscieme, A. S. Golden, C. A. Guerra, U. Jacob, Y. Takahashi, J. Settele, S. Díaz, Z. Molnár, A. Purvis, The direct drivers of recent global anthropogenic biodiversity loss. *Sci. Adv.* **8**, eabm9982 (2022). doi:10.1126/sciadv.abm9982 Medline

7. J. Huang, X. Zhang, Q. Zhang, Y. Lin, M. Hao, Y. Luo, Z. Zhao, Y. Yao, X. Chen, L. Wang, S. Nie, Y. Yin, Y. Xu, J. Zhang, Recently amplified arctic warming has contributed to a continental global warming trend. *Nat. Clim. Chang.* **7**, 875–879 (2017). doi:10.1038/s41558-017-0009-5

8. M. Macias-Fauria, P. Jepson, N. Zimov, Y. Malhi, Pleistocene Arctic megafaunal ecological engineering as a natural climate solution? *Phil. Trans. R. Soc. B* **375**, 20190122 (2020). doi:10.1098/rstb.2019.0122 Medline

9. W. J. Ripple, G. Chapron, J. V. López-Bao, S. M. Durant, D. W. Macdonald, P. A. Lindsey, E. L. Bennett, R. L. Beschta, J. T. Bruskotter, A. Campos-Arceiz, R. T. Corlett, C. T. Darimont, A. J. Dickman, R. Dirzo, H. T. Dublin, J. A. Estes, K. T. Everatt, M. Galetti, V. R. Goswami, M. W. Hayward, S. Hedges, M. Hoffmann, L. T. B. Hunter, G. I. H. Kerley, M. Letnic, T. Levi, F. Maisels, J. C. Morrison, M. P. Nelson, T. M. Newsome, L. Painter, R. M. Pringle, C. J. Sandom, J. Terborgh, A. Treves, B. Van Valkenburgh, J. A. Vucetich, A. J. Wirsing, A. D. Wallach, C. Wolf, R. Woodroffe, H. Young, L. Zhang, Conserving the world's megafauna and biodiversity: The fierce urgency of now. *Bioscience* **67**, 197–200 (2017). doi:10.1093/biosci/biw168

10. R. E. Morlan, J. Cinq-Mars, in *Paleoecology of Beringia*, D. M. Hopkins, J. V. Matthews, C. E. Schweger, S. B. Young, Eds. (Academic Press, 1982), pp. 353–381.

11. E. Y. Pavlova, V. V. Pitulko, Late Pleistocene and Early Holocene climate changes and human habitation in the arctic Western Beringia based on revision of palaeobotanical data. *Quat. Int.* **549**, 5–25 (2020). doi:10.1016/j.quaint.2020.04.015

12. J. A. Swift, M. Bunce, J. Dortch, K. Douglass, J. T. Faith, J. A. Fellows Yates, J. Field, S. G. Haberle, E. Jacob, C. N. Johnson, E. Lindsey, E. D. Lorenzen, J. Louys, G. Miller, A. M. Mychajliw, V. Slon, N. A. Villavicencio, M. R. Waters, F. Welker, R. Wood, M. Petraglia, N. Boivin, P. Roberts, Micro methods for megafauna: Novel approaches to Late Quaternary extinctions and their contributions to faunal conservation in the Anthropocene. *Bioscience* **69**, 877–887 (2019). doi:10.1093/biosci/biz105 Medline

13. D. H. Mann, P. Groves, R. E. Reanier, B. V. Gaglioti, M. L. Kunz, B. Shapiro, Life and extinction of megafauna in the ice-age Arctic. *Proc. Natl. Acad. Sci. U.S.A.* **112**, 14301–14306 (2015). doi:10.1073/pnas.1516573112 Medline

14. M. Stewart, W. C. Carleton, H. S. Groucutt, Climate change, not human population growth, correlates with Late Quaternary megafauna declines in North America. *Nat. Commun.* **12**, 965 (2021). doi:10.1038/s41467-021-21201-8 Medline

15. E. J. Gowan, X. Zhang, S. Khosravi, A. Rovere, P. Stocchi, A. L. C. Hughes, R. Gyllencreutz, J. Mangerud, J.-I. Svendsen, G. Lohmann, A new global ice sheet reconstruction for the past 80 000 years. *Nat. Commun.* **12**, 1199 (2021). doi:10.1038/s41467-021-21469-w Medline

16. C. D. Clark, J. C. Ely, R. C. A. Hindmarsh, S. Bradley, A. Ignéczi, D. Fabel, C. Ó Cofaigh, R. C. Chiverrell, J. Scourse, S. Benetti, T. Bradwell, D. J. A. Evans, D. H. Roberts, M. Burke, S. L. Callard, A. Medialdea, M. Saher, D. Small, R. K. Smedley, E. Gasson, L. Gregoire, N. Gandy, A. L. C. Hughes, C. Ballantyne, M. D. Bateman, G. R. Bigg, J. Doole, D. Dove, G. A. T. Duller, G. T. H. Jenkins, S. L. Livingstone, S. McCarron, S. Moreton, D. Pollard, D. Praeg, H. P. Sejrup, K. J. J. Van Landeghem, P. Wilson, Growth and retreat of the last British–Irish Ice Sheet, 31 000 to 15 000 years ago: The BRITICE-CHRONO reconstruction. *Boreas* **51**, 699–758 (2022). doi:10.1111/bor.12594

17. J. R. Farmer, T. Pico, O. M. Underwood, R. Cleveland Stout, J. Granger, T. M. Cronin, F. Fripiat, A. Martínez-García, G. H. Haug, D. M. Sigman, The Bering Strait was flooded 10,000 years before the Last Glacial Maximum. *Proc. Natl. Acad. Sci. U.S.A.* **120**, e2206742119 (2023). doi:10.1073/pnas.2206742119 Medline

18. J. W. Williams, B. N. Shuman, T. Webb III, P. J. Bartlein, P. L. Leduc, Late-Quaternary vegetation dynamics in North America: Scaling from taxa to biomes. *Ecol. Monogr.* **74**, 309–334 (2004). doi:10.1890/02-4045

19. M. T. Rabanus-Wallace, M. J. Wooller, G. D. Zazula, E. Shute, A. H. Jahren, P. Kosintsev, J. A. Burns, J. Breen, B. Llamas, A. Cooper, Megafaunal isotopes reveal role of increased moisture on rangeland during late Pleistocene extinctions. *Nat. Ecol. Evol.* **1**, 0125 (2017). doi:10.1038/s41559-017-0125 Medline

20. E. D. Lorenzen, D. Nogués-Bravo, L. Orlando, J. Weinstock, J. Binladen, K. A. Marske, A. Ugan, M. K. Borregaard, M. T. P. Gilbert, R. Nielsen, S. Y. W. Ho, T. Goebel, K. E. Graf, D. Byers, J. T. Stenderup, M. Rasmussen, P. F. Campos, J. A. Leonard, K.-P. Koepfli, D. Froese, G. Zazula, T. W. Stafford Jr., K. Aaris-Sørensen, P. Batra, A. M. Haywood, J. S. Singarayer, P. J. Valdes, G. Boeskorov, J. A. Burns, S. P. Davydov, J. Haile, D. L. Jenkins, P. Kosintsev, T. Kuznetsova, X. Lai, L. D. Martin, H. G. McDonald,

D. Mol, M. Meldgaard, K. Munch, E. Stephan, M. Sablin, R. S. Sommer, T. Sipko, E. Scott, M. A. Suchard, A. Tikhonov, R. Willerslev, R. K. Wayne, A. Cooper, M. Hofreiter, A. Sher, B. Shapiro, C. Rahbek, E. Willerslev, Species-specific responses of Late Quaternary megafauna to climate and humans. *Nature* **479**, 359–364 (2011). doi:10.1038/nature10574 Medline

21. P. D. Heintzman, G. D. Zazula, R. MacPhee, E. Scott, J. A. Cahill, B. K. McHorse, J. D. Kapp, M. Stiller, M. J. Wooller, L. Orlando, J. Southon, D. G. Froese, B. Shapiro, A new genus of horse from Pleistocene North America. *eLife* **6**, e29944 (2017). doi:10.7554/eLife.29944 Medline

22. A. O. Vershinina, P. D. Heintzman, D. G. Froese, G. Zazula, M. Cassatt-Johnstone, L. Dalén, C. Der Sarkissian, S. G. Dunn, L. Ermini, C. Gamba, P. Groves, J. D. Kapp, D. H. Mann, A. Seguin-Orlando, J. Southon, M. Stiller, M. J. Wooller, G. Baryshnikov, D. Gimranov, E. Scott, E. Hall, S. Hewitson, I. Kirillova, P. Kosintsev, F. Shidlovsky, H.-W. Tong, M. P. Tiunov, S. Vartanyan, L. Orlando, R. Corbett-Detig, R. D. MacPhee, B. Shapiro, Ancient horse genomes reveal the timing and extent of dispersals across the Bering Land Bridge. *Mol. Ecol.* **30**, 6144–6161 (2021). doi:10.1111/mec.15977 Medline

23. C. R. Harington, Pleistocene vertebrates of the Yukon Territory. *Quat. Sci. Rev.* **30**, 2341–2354 (2011). doi:10.1016/j.quascirev.2011.05.020

24. L. Orlando, The evolutionary and historical foundation of the modern horse: Lessons from ancient genomics. *Annu. Rev. Genet.* **54**, 563–581 (2020). doi:10.1146/annurev-genet-021920-011805 Medline

25. P. Librado, G. Tressières, L. Chauvey, A. Fages, N. Khan, S. Schiavinato, L. Calvière-Tonasso, M. A. Kusliy, C. Gaunitz, X. Liu, S. Wagner, C. Der Sarkissian, A. Seguin-Orlando, A. Perdereau, J.-M. Aury, J. Southon, B. Shapiro, O. Bouchez, C. Donnadieu, Y. R. H. Collin, K. M. Gregersen, M. D. Jessen, K. Christensen, L. Claudi-Hansen, M. Pruvost, E. Pucher, H. Vulic, M. Novak, A. Rimpf, P. Turk, S. Reiter, G. Brem, C. Schwall, É. Barrey, C. Robert, C. Degueurce, L. K. Horwitz, L. Klassen, U. Rasmussen, J. Kveiborg, N. N. Johannsen, D. Makowiecki, P. Makarowicz, M. Szeliga, V. Ilchyshyn, V. Rud, J. Romaniszyn, V. E. Mullin, M. Verdugo, D. G. Bradley, J. L. Cardoso, M. J. Valente, M. Telles Antunes, C. Ameen, R. Thomas, A. Ludwig, M. Marzullo, O. Prato, G. Bagnasco Gianni, U. Tecchiati, J. Granado, A. Schlumbaum, S. Deschler-Erb, M. S. Mráz, N. Boulbes, A. Gardeisen, C. Mayer, H.-J. Döhle, M. Vicze, P. A. Kosintsev, R. Kyselý, L. Peške, T. O'Connor, E. Ananyevskaya, I. Shevnina, A. Logvin, A. A. Kovalev, T.-O. Iderkhangai, M. V. Sablin, P. K. Dashkovskiy, A. S. Graphodatsky, I. Merts, V. Merts, A. K. Kasparov, V. V. Pitulko, V. Onar, A. Öztan, B. S. Arbuckle, H. McColl, G. Renaud, R. Khaskhanov, S. Demidenko, A. Kadieva, B. Atabiev, M. Sundqvist, G. Lindgren, F. J. López-Cachero, S. Albizuri, T. Trbojević Vukičević, A. Rapan Papeša, M. Burić, P. Rajić Šikanjić, J. Weinstock, D. Asensio Vilaró, F. Codina, C. García Dalmau, J. Morer de Llorens, J. Pou, G. de Prado, J. Sanmartí, N. Kallala, J. R. Torres, B. Maraoui-Telmini, M.-C. Belarte Franco, S. Valenzuela-Lamas, A. Zazzo, S. Lepetz, S. Duchesne, A. Alexeev, J. Bayarsaikhan, J.-L. Houle, N. Bayarkhuu, T. Turbat, É. Crubézy, I. Shingiray, M. Mashkour, N. Y. Berezina, D. S. Korobov, A. Belinskiy, A. Kalmykov, J.-P. Demoule, S. Reinhold, S. Hansen, B. Wallner, N. Roslyakova, P. F. Kuznetsov, A. A. Tishkin, P. Wincker, K. Kanne, A. Outram, L. Orlando, Widespread

horse-based mobility arose around 2200 BCE in Eurasia. *Nature* **631**, 819–825 (2024). doi:10.1038/s41586-024-07597-5 Medline

26. W. T. T. Taylor, P. Librado, C. J. American Horse, C. Shield Chief Gover, J. Arterberry, A. L. Afraid of Bear-Cook, H. Left Heron, R. M. Yellow Hair, M. Gonzalez, B. Means, S. High Crane, W. W. Yellow Bull, B. Dull Knife, A. Afraid of Bear, C. Tecumseh Collin, C. Ward, T. A. Pasqual, L. Chauvey, L. Tonasso-Calviere, S. Schiavinato, A. Seguin-Orlando, A. Fages, N. Khan, C. Der Sarkissian, X. Liu, S. Wagner, B. G. Leonard, B. L. Manzano, N. O'Malley, J. A. Leonard, E. Bernáldez-Sánchez, E. Barrey, L. Charliquart, E. Robbe, T. Denoblet, K. Gregersen, A. O. Vershinina, J. Weinstock, P. Rajić Šikanjić, M. Mashkour, I. Shingiray, J. M. Aury, A. Perdereau, S. Alquraishi, A. H. Alfarhan, K. A. S. Al-Rasheid, T. Trbojević Vukičević, M. Buric, E. Sauer, M. Lucas, J. Brenner-Coltrain, J. R. Bozell, C. A. Thornhill, V. Monagle, A. Perri, C. Newton, W. E. Hall, J. L. Conver, P. Le Roux, S. G. Buckser, C. Gabe, J. B. Belardi, C. I. Barrón-Ortiz, I. A. Hart, C. Ryder, M. Sponheimer, B. Shapiro, J. Southon, J. Hibbs, C. Faulkner, A. Outram, L. Patterson Rosa, K. Palermo, M. Solé, A. William, W. McCrory, G. Lindgren, S. Brooks, C. Eché, C. Donnadieu, O. Bouchez, P. Wincker, G. Hodgins, S. Trabert, B. Bethke, P. Roberts, E. L. Jones, Y. Running Horse Collin, L. Orlando, Early dispersal of domestic horses into the Great Plains and northern Rockies. *Science* **379**, 1316–1323 (2023). doi:10.1126/science.adc9691 Medline

27. J. Yuan, G. Sheng, M. Preick, B. Sun, X. Hou, S. Chen, U. H. Taron, A. Barlow, L. Wang, J. Hu, T. Deng, X. Lai, M. Hofreiter, Mitochondrial genomes of Late Pleistocene caballine horses from China belong to a separate clade. *Quat. Sci. Rev.* **250**, 106691 (2020). doi:10.1016/j.quascirev.2020.106691

28. B. J. MacFadden, O. Carranza-Castañeda, Cranium of *Dinohippus mexicanus* (Mammalia: Equidae) from the early Pliocene (latest Hemphillian) of central Mexico, and the origin of *Equus*. *Bull. Fla. Mus. Nat. Hist.* **43**, 163–185 (2002). doi:10.58782/flmnh.tsom4551

29. D. H. Alexander, J. Novembre, K. Lange, Fast model-based estimation of ancestry in unrelated individuals. *Genome Res.* **19**, 1655–1664 (2009). doi:10.1101/gr.094052.109 Medline

30. N. Patterson, P. Moorjani, Y. Luo, S. Mallick, N. Rohland, Y. Zhan, T. Genschoreck, T. Webster, D. Reich, Ancient admixture in human history. *Genetics* **192**, 1065–1093 (2012). doi:10.1534/genetics.112.145037 Medline

31. P. Librado, L. Orlando, Struct-f4: A Rcpp package for ancestry profile and population structure inference from f_4-statistics. *Bioinformatics* **38**, 2070–2071 (2022). doi:10.1093/bioinformatics/btac046 Medline

32. S. V. Nielsen, A. H. Vaughn, K. Leppälä, M. J. Landis, T. Mailund, R. Nielsen, Bayesian inference of admixture graphs on Native American and Arctic populations. *PLOS Genet.* **19**, e1010410 (2023). doi:10.1371/journal.pgen.1010410 Medline

33. E. K. Molloy, A. Durvasula, S. Sankararaman, Advancing admixture graph estimation via maximum likelihood network orientation. *Bioinformatics* **37**, i142–i150 (2021). doi:10.1093/bioinformatics/btab267 Medline

34. E. Santiago, I. Novo, A. F. Pardiñas, M. Saura, J. Wang, A. Caballero, Recent demographic history inferred by high-resolution analysis of Linkage Disequilibrium. *Mol. Biol. Evol.* **37**, 3642–3653 (2020). doi:10.1093/molbev/msaa169 Medline

35. G. M. MacDonald, T. K. McLeod, The Holocene closing of the 'ice-free' corridor: A biogeographical perspective. *Quat. Int.* **32**, 87–95 (1996). doi:10.1016/1040-6182(95)00055-0

36. C. I. Barrón-Ortiz, C. N. Jass, R. Barrón-Corvera, J. Austen, J. M. Theodor, Enamel hypoplasia and dental wear of North American late Pleistocene horses and bison: An assessment of nutritionally based extinction models. *Paleobiology* **45**, 484–515 (2019). doi:10.1017/pab.2019.17

37. M. Schubert, H. Jónsson, D. Chang, C. Der Sarkissian, L. Ermini, A. Ginolhac, A. Albrechtsen, I. Dupanloup, A. Foucal, B. Petersen, M. Fumagalli, M. Raghavan, A. Seguin-Orlando, T. S. Korneliussen, A. M. V. Velazquez, J. Stenderup, C. A. Hoover, C.-J. Rubin, A. H. Alfarhan, S. A. Alquraishi, K. A. S. Al-Rasheid, D. E. MacHugh, T. Kalbfleisch, J. N. MacLeod, E. M. Rubin, T. Sicheritz-Ponten, L. Andersson, M. Hofreiter, T. Marques-Bonet, M. T. P. Gilbert, R. Nielsen, L. Excoffier, E. Willerslev, B. Shapiro, L. Orlando, Prehistoric genomes reveal the genetic foundation and cost of horse domestication. *Proc. Natl. Acad. Sci. U.S.A.* **111**, E5661–E5669 (2014). doi:10.1073/pnas.1416991111 Medline

38. A. Fages, K. Hanghøj, N. Khan, C. Gaunitz, A. Seguin-Orlando, M. Leonardi, C. McCrory Constantz, C. Gamba, K. A. S. Al-Rasheid, S. Albizuri, A. H. Alfarhan, M. Allentoft, S. Alquraishi, D. Anthony, N. Baimukhanov, J. H. Barrett, J. Bayarsaikhan, N. Benecke, E. Bernáldez-Sánchez, L. Berrocal-Rangel, F. Biglari, S. Boessenkool, B. Boldgiv, G. Brem, D. Brown, J. Burger, E. Crubézy, L. Daugnora, H. Davoudi, P. de Barros Damgaard, M. de Los Ángeles de Chorro Y de Villa-Ceballos, S. Deschler-Erb, C. Detry, N. Dill, M. do Mar Oom, A. Dohr, S. Ellingvåg, D. Erdenebaatar, H. Fathi, S. Felkel, C. Fernández-Rodríguez, E. García-Viñas, M. Germonpré, J. D. Granado, J. H. Hallsson, H. Hemmer, M. Hofreiter, A. Kasparov, M. Khasanov, R. Khazaeli, P. Kosintsev, K. Kristiansen, T. Kubatbek, L. Kuderna, P. Kuznetsov, H. Laleh, J. A. Leonard, J. Lhuillier, C. Liesau von Lettow-Vorbeck, A. Logvin, L. Lõugas, A. Ludwig, C. Luis, A. M. Arruda, T. Marques-Bonet, R. Matoso Silva, V. Merz, E. Mijiddorj, B. K. Miller, O. Monchalov, F. A. Mohaseb, A. Morales, A. Nieto-Espinet, H. Nistelberger, V. Onar, A. H. Pálsdóttir, V. Pitulko, K. Pitskhelauri, M. Pruvost, P. Rajic Sikanjic, A. Rapan Papeša, N. Roslyakova, A. Sardari, E. Sauer, R. Schafberg, A. Scheu, J. Schibler, A. Schlumbaum, N. Serrand, A. Serres-Armero, B. Shapiro, S. Sheikhi Seno, I. Shevnina, S. Shidrang, J. Southon, B. Star, N. Sykes, K. Taheri, W. Taylor, W.-R. Teegen, T. Trbojević Vukičević, S. Trixl, D. Tumen, S. Undrakhbold, E. Usmanova, A. Vahdati, S. Valenzuela-Lamas, C. Viegas, B. Wallner, J. Weinstock, V. Zaibert, B. Clavel, S. Lepetz, M. Mashkour, A. Helgason, K. Stefánsson, E. Barrey, E. Willerslev, A. K. Outram, P. Librado, L. Orlando, Tracking Five Millennia of Horse Management with Extensive Ancient Genome Time Series. *Cell* **177**, 1419–1435.e31 (2019). doi:10.1016/j.cell.2019.03.049 Medline

39. P. Librado, C. Der Sarkissian, L. Ermini, M. Schubert, H. Jónsson, A. Albrechtsen, M. Fumagalli, M. A. Yang, C. Gamba, A. Seguin-Orlando, C. D. Mortensen, B. Petersen, C. A. Hoover, B. Lorente-Galdos, A. Nedoluzhko, E. Boulygina, S. Tsygankova, M. Neuditschko, V. Jagannathan, C. Thèves, A. H. Alfarhan, S. A. Alquraishi, K. A. S. Al-Rasheid, T. Sicheritz-Ponten, R. Popov, S. Grigoriev, A. N. Alekseev, E. M. Rubin, M. McCue, S. Rieder, T. Leeb, A. Tikhonov, E. Crubézy, M. Slatkin, T. Marques-Bonet, R. Nielsen, E. Willerslev, J. Kantanen, E. Prokhortchouk, L. Orlando, Tracking the origins

of Yakutian horses and the genetic basis for their fast adaptation to subarctic environments. *Proc. Natl. Acad. Sci. U.S.A.* **112**, E6889–E6897 (2015). doi:10.1073/pnas.1513696112 Medline

40. D. Froese, M. Stiller, P. D. Heintzman, A. V. Reyes, G. D. Zazula, A. E. R. Soares, M. Meyer, E. Hall, B. J. L. Jensen, L. J. Arnold, R. D. E. MacPhee, B. Shapiro, Fossil and genomic evidence constrains the timing of bison arrival in North America. *Proc. Natl. Acad. Sci. U.S.A.* **114**, 3457–3462 (2017). doi:10.1073/pnas.1620754114 Medline

41. R. D. Guthrie, *Frozen Fauna of the Mammoth Steppe: The Story of Blue Babe* (Univ. Chicago Press, 1990).

42. S. A. Zimov, N. S. Zimov, A. N. Tikhonov, F. S. Chapin III, Mammoth steppe: A high-productivity phenomenon. *Quat. Sci. Rev.* **57**, 26–45 (2012). doi:10.1016/j.quascirev.2012.10.005

43. A. S. Dalton, H. E. Dulfer, M. Margold, J. Heyman, J. J. Clague, D. G. Froese, M. S. Gauthier, A. L. C. Hughes, C. E. Jennings, S. L. Norris, B. J. Stoker, Deglaciation of the North American ice sheet complex in calendar years based on a comprehensive database of chronological data: NADI-1. *Quat. Sci. Rev.* **321**, 108345 (2023). doi:10.1016/j.quascirev.2023.108345

44. P. F. Campos, E. Willerslev, A. Sher, L. Orlando, E. Axelsson, A. Tikhonov, K. Aaris-Sørensen, A. D. Greenwood, R.-D. Kahlke, P. Kosintsev, T. Krakhmalnaya, T. Kuznetsova, P. Lemey, R. MacPhee, C. A. Norris, K. Shepherd, M. A. Suchard, G. D. Zazula, B. Shapiro, M. T. P. Gilbert, Ancient DNA analyses exclude humans as the driving force behind late Pleistocene musk ox (*Ovibos moschatus*) population dynamics. *Proc. Natl. Acad. Sci. U.S.A.* **107**, 5675–5680 (2010). doi:10.1073/pnas.0907189107 Medline

45. A. G. Rowe, C. P. Bataille, S. Baleka, E. A. Combs, B. A. Crass, D. C. Fisher, S. Ghosh, C. E. Holmes, K. E. Krasinski, F. Lanoë, T. J. Murchie, H. Poinar, B. Potter, J. T. Rasic, J. Reuther, G. M. Smith, K. J. Spaleta, B. T. Wygal, M. J. Wooller, A female woolly mammoth's lifetime movements end in an ancient Alaskan hunter-gatherer camp. *Sci. Adv.* **10**, eadk0818 (2024). doi:10.1126/sciadv.adk0818 Medline

46. A. D. Barnosky, P. L. Koch, R. S. Feranec, S. L. Wing, A. B. Shabel, Assessing the causes of late Pleistocene extinctions on the continents. *Science* **306**, 70–75 (2004). doi:10.1126/science.1101476 Medline

47. M. Meiri, A. M. Lister, M. J. Collins, N. Tuross, T. Goebel, S. Blockley, G. D. Zazula, N. van Doorn, R. Dale Guthrie, G. G. Boeskorov, G. F. Baryshnikov, A. Sher, I. Barnes, Faunal record identifies Bering isthmus conditions as constraint to end-Pleistocene migration to the New World. *Proc. R. Soc. B* **281**, 20132167 (2014). doi:10.1098/rspb.2013.2167 Medline

48. M. Meiri, A. Lister, P. Kosintsev, G. Zazula, I. Barnes, Population dynamics and range shifts of moose (*Alces alces*) during the Late Quaternary. *J. Biogeogr.* **47**, 2223–2234 (2020). doi:10.1111/jbi.13935

49. D. Guo, H. Wang, V. E. Romanovsky, A. M. Haywood, N. Pepin, U. Salzmann, J. Sun, Q. Yan, Z. Zhang, X. Li, B. L. Otto-Bliesner, R. Feng, G. Lohmann, C. Stepanek, A. Abe-Ouchi, W.-L. Chan, W. R. Peltier, D. Chandan, A. S. von der Heydt, C. Contoux, M. A.

Chandler, N. Tan, Q. Zhang, S. J. Hunter, Y. Kamae, Highly restricted near-surface permafrost extent during the mid-Pliocene warm period. *Proc. Natl. Acad. Sci. U.S.A.* **120**, e2301954120 (2023). doi:10.1073/pnas.2301954120 Medline

50. A. Lindgren, G. Hugelius, P. Kuhry, T. R. Christensen, J. Vandenberghe, GIS-based maps and area estimates of northern hemisphere permafrost extent during the Last Glacial Maximum. *Permafrost Periglac. Process.* **27**, 6–16 (2016). doi:10.1002/ppp.1851

51. P. Kindler, M. Guillevic, M. Baumgartner, J. Schwander, A. Landais, M. Leuenberger, Temperature reconstruction from 10 to 120 kyr b2k from the NGRIP ice core. *Clim. Past* **10**, 887–902 (2014). doi:10.5194/cp-10-887-2014

52. C. Bataille, L. Orlando, Following Late Pleistocene horse migration toward our sustainable future, Open Science Framework (2025). doi:10.17605/OSF.IO/Z2XT4

53. E. T. Todd, L. Tonasso-Calvière, L. Chauvey, S. Schiavinato, A. Fages, A. Seguin-Orlando, P. Clavel, N. Khan, L. Pérez Pardal, L. Patterson Rosa, P. Librado, H. Ringbauer, M. Verdugo, J. Southon, J.-M. Aury, A. Perdereau, E. Vila, M. Marzullo, O. Prato, U. Tecchiati, G. Bagnasco Gianni, A. Tagliacozzo, V. Tinè, F. Alhaique, J. L. Cardoso, M. J. Valente, M. Telles Antunes, L. Frantz, B. Shapiro, D. G. Bradley, N. Boulbes, A. Gardeisen, L. K. Horwitz, A. Öztan, B. S. Arbuckle, V. Onar, B. Clavel, S. Lepetz, A. A. Vahdati, H. Davoudi, A. Mohaseb, M. Mashkour, O. Bouchez, C. Donnadieu, P. Wincker, S. A. Brooks, A. Beja-Pereira, D.-D. Wu, L. Orlando, The genomic history and global expansion of domestic donkeys. *Science* **377**, 1172–1180 (2022). doi:10.1126/science.abo3503 Medline

54. P. Librado, N. Khan, A. Fages, M. A. Kusliy, T. Suchan, L. Tonasso-Calvière, S. Schiavinato, D. Alioglu, A. Fromentier, A. Perdereau, J.-M. Aury, C. Gaunitz, L. Chauvey, A. Seguin-Orlando, C. Der Sarkissian, J. Southon, B. Shapiro, A. A. Tishkin, A. A. Kovalev, S. Alquraishi, A. H. Alfarhan, K. A. S. Al-Rasheid, T. Seregély, L. Klassen, R. Iversen, O. Bignon-Lau, P. Bodu, M. Olive, J.-C. Castel, M. Boudadi-Maligne, N. Alvarez, M. Germonpré, M. Moskal-Del Hoyo, J. Wilczyński, S. Pospuła, A. Lasota-Kuś, K. Tunia, M. Nowak, E. Rannamäe, U. Saarma, G. Boeskorov, L. Lõugas, R. Kyselý, L. Peške, A. Bălăşescu, V. Dumitraşcu, R. Dobrescu, D. Gerber, V. Kiss, A. Szécsényi-Nagy, B. G. Mende, Z. Gallina, K. Somogyi, G. Kulcsár, E. Gál, R. Bendrey, M. E. Allentoft, G. Sirbu, V. Dergachev, H. Shephard, N. Tomadini, S. Grouard, A. Kasparov, A. E. Basilyan, M. A. Anisimov, P. A. Nikolskiy, E. Y. Pavlova, V. Pitulko, G. Brem, B. Wallner, C. Schwall, M. Keller, K. Kitagawa, A. N. Bessudnov, A. Bessudnov, W. Taylor, J. Magail, J.-O. Gantulga, J. Bayarsaikhan, D. Erdenebaatar, K. Tabaldiev, E. Mijiddorj, B. Boldgiv, T. Tsagaan, M. Pruvost, S. Olsen, C. A. Makarewicz, S. Valenzuela Lamas, S. Albizuri Canadell, A. Nieto Espinet, M. P. Iborra, J. Lira Garrido, E. Rodríguez González, S. Celestino, C. Olària, J. L. Arsuaga, N. Kotova, A. Pryor, P. Crabtree, R. Zhumatayev, A. Toleubaev, N. L. Morgunova, T. Kuznetsova, D. Lordkipanize, M. Marzullo, O. Prato, G. Bagnasco Gianni, U. Tecchiati, B. Clavel, S. Lepetz, H. Davoudi, M. Mashkour, N. Y. Berezina, P. W. Stockhammer, J. Krause, W. Haak, A. Morales-Muñiz, N. Benecke, M. Hofreiter, A. Ludwig, A. S. Graphodatsky, J. Peters, K. Y. Kiryushin, T.-O. Iderkhangai, N. A. Bokovenko, S. K. Vasiliev, N. N. Seregin, K. V. Chugunov, N. A. Plasteeva, G. F. Baryshnikov, E. Petrova, M. Sablin, E. Ananyevskaya, A. Logvin, I. Shevnina, V. Logvin, S. Kalieva, V. Loman, I. Kukushkin, I. Merz, V. Merz, S. Sakenov, V. Varfolomeyev, E. Usmanova, V. Zaibert, B. Arbuckle,

A. B. Belinskiy, A. Kalmykov, S. Reinhold, S. Hansen, A. I. Yudin, A. A. Vybornov, A. Epimakhov, N. S. Berezina, N. Roslyakova, P. A. Kosintsev, P. F. Kuznetsov, D. Anthony, G. J. Kroonen, K. Kristiansen, P. Wincker, A. Outram, L. Orlando, The origins and spread of domestic horses from the Western Eurasian steppes. *Nature* **598**, 634–640 (2021). doi:10.1038/s41586-021-04018-9 Medline

55. P. Korlević, M. Meyer, Pretreatment: Removing DNA Contamination from Ancient Bones and Teeth Using Sodium Hypochlorite and Phosphate. *Methods Mol. Biol.* **1963**, 15–19 (2019). doi:10.1007/978-1-4939-9176-1_2 Medline

56. J. Dabney, M. Meyer, Extraction of Highly Degraded DNA from Ancient Bones and Teeth. *Methods Mol. Biol.* **1963**, 25–29 (2019). doi:10.1007/978-1-4939-9176-1_4 Medline

57. J. D. Kapp, R. E. Green, B. Shapiro, A Fast and Efficient Single-stranded Genomic Library Preparation Method Optimized for Ancient DNA. *J. Hered.* **112**, 241–249 (2021). doi:10.1093/jhered/esab012 Medline

58. B. Sundararaman, A. O. Vershinina, S. Hershauer, J. D. Kapp, S. Dunn, B. Shapiro, R. E. Green, A method to generate capture baits for targeted sequencing. *Nucleic Acids Res.* **51**, e69 (2023). doi:10.1093/nar/gkad460 Medline

59. L. Orlando, A. Ginolhac, G. Zhang, D. Froese, A. Albrechtsen, M. Stiller, M. Schubert, E. Cappellini, B. Petersen, I. Moltke, P. L. F. Johnson, M. Fumagalli, J. T. Vilstrup, M. Raghavan, T. Korneliussen, A.-S. Malaspinas, J. Vogt, D. Szklarczyk, C. D. Kelstrup, J. Vinther, A. Dolocan, J. Stenderup, A. M. V. Velazquez, J. Cahill, M. Rasmussen, X. Wang, J. Min, G. D. Zazula, A. Seguin-Orlando, C. Mortensen, K. Magnussen, J. F. Thompson, J. Weinstock, K. Gregersen, K. H. Røed, V. Eisenmann, C. J. Rubin, D. C. Miller, D. F. Antczak, M. F. Bertelsen, S. Brunak, K. A. S. Al-Rasheid, O. Ryder, L. Andersson, J. Mundy, A. Krogh, M. T. P. Gilbert, K. Kjær, T. Sicheritz-Ponten, L. J. Jensen, J. V. Olsen, M. Hofreiter, R. Nielsen, B. Shapiro, J. Wang, E. Willerslev, Recalibrating *Equus* evolution using the genome sequence of an early Middle Pleistocene horse. *Nature* **499**, 74–78 (2013). doi:10.1038/nature12323 Medline

60. M. Schubert, S. Lindgreen, L. Orlando, AdapterRemoval v2: Rapid adapter trimming, identification, and read merging. *BMC Res. Notes* **9**, 88 (2016). doi:10.1186/s13104-016-1900-2 Medline

61. T. S. Kalbfleisch, E. S. Rice, M. S. DePriest Jr., B. P. Walenz, M. S. Hestand, J. R. Vermeesch, B. L. O'Connell, I. T. Fiddes, A. O. Vershinina, N. F. Saremi, J. L. Petersen, C. J. Finno, R. R. Bellone, M. E. McCue, S. A. Brooks, E. Bailey, L. Orlando, R. E. Green, D. C. Miller, D. F. Antczak, J. N. MacLeod, Improved reference genome for the domestic horse increases assembly contiguity and composition. *Commun. Biol.* **1**, 197 (2018). doi:10.1038/s42003-018-0199-z Medline

62. S. Felkel, C. Vogl, D. Rigler, V. Dobretsberger, B. P. Chowdhary, O. Distl, R. Fries, V. Jagannathan, J. E. Janečka, T. Leeb, G. Lindgren, M. McCue, J. Metzger, M. Neuditschko, T. Rattei, T. Raudsepp, S. Rieder, C.-J. Rubin, R. Schaefer, C. Schlötterer, G. Thaller, J. Tetens, B. Velie, G. Brem, B. Wallner, The horse Y chromosome as an informative marker for tracing sire lines. *Sci. Rep.* **9**, 6095 (2019). doi:10.1038/s41598-019-42640-w Medline

63. M. Schubert, L. Ermini, C. Der Sarkissian, H. Jónsson, A. Ginolhac, R. Schaefer, M. D. Martin, R. Fernández, M. Kircher, M. McCue, E. Willerslev, L. Orlando,

Characterization of ancient and modern genomes by SNP detection and phylogenomic and metagenomic analysis using PALEOMIX. *Nat. Protoc.* **9**, 1056–1082 (2014). doi:10.1038/nprot.2014.063 Medline

64. B. Langmead, S. L. Salzberg, Fast gapped-read alignment with Bowtie 2. *Nat. Methods* **9**, 357–359 (2012). doi:10.1038/nmeth.1923 Medline

65. M. Poullet, L. Orlando, Assessing DNA sequence alignment methods for characterizing ancient genomes and methylomes. *Front. Ecol. Evol.* **8**, 105 (2020). doi:10.3389/fevo.2020.00105

66. A. McKenna, M. Hanna, E. Banks, A. Sivachenko, K. Cibulskis, A. Kernytsky, K. Garimella, D. Altshuler, S. Gabriel, M. Daly, M. A. DePristo, The Genome Analysis Toolkit: A MapReduce framework for analyzing next-generation DNA sequencing data. *Genome Res.* **20**, 1297–1303 (2010). doi:10.1101/gr.107524.110 Medline

67. P. Skoglund, B. H. Northoff, M. V. Shunkov, A. P. Derevianko, S. Pääbo, J. Krause, M. Jakobsson, Separating endogenous ancient DNA from modern day contamination in a Siberian Neandertal. *Proc. Natl. Acad. Sci. U.S.A.* **111**, 2229–2234 (2014). doi:10.1073/pnas.1318934111 Medline

68. H. Jónsson, A. Ginolhac, M. Schubert, P. L. Johnson, L. Orlando, mapDamage2.0: Fast approximate Bayesian estimates of ancient DNA damage parameters. *Bioinformatics* **29**, 1682–1684 (2013). doi:10.1093/bioinformatics/btt193 Medline

69. L. Orlando, R. Allaby, P. Skoglund, C. Der Sarkissian, P. W. Stockhammer, M. C. Ávila-Arcos, Q. Fu, J. Krause, E. Willerslev, A. C. Stone, C. Warinner, Ancient DNA analysis. *Nat. Rev. Methods Primers* **1**, 14 (2021). doi:10.1038/s43586-020-00011-0

70. J. S. Pedersen, E. Valen, A. M. V. Velazquez, B. J. Parker, M. Rasmussen, S. Lindgreen, B. Lilje, D. J. Tobin, T. K. Kelly, S. Vang, R. Andersson, P. A. Jones, C. A. Hoover, A. Tikhonov, E. Prokhortchouk, E. M. Rubin, A. Sandelin, M. T. P. Gilbert, A. Krogh, E. Willerslev, L. Orlando, Genome-wide nucleosome map and cytosine methylation levels of an ancient human genome. *Genome Res.* **24**, 454–466 (2014). doi:10.1101/gr.163592.113 Medline

71. A. W. Briggs, U. Stenzel, P. L. F. Johnson, R. E. Green, J. Kelso, K. Prüfer, M. Meyer, J. Krause, M. T. Ronan, M. Lachmann, S. Pääbo, Patterns of damage in genomic DNA sequences from a Neandertal. *Proc. Natl. Acad. Sci. U.S.A.* **104**, 14616–14621 (2007). doi:10.1073/pnas.0704665104 Medline

72. T. S. Korneliussen, I. Moltke, A. Albrechtsen, R. Nielsen, Calculation of Tajima's *D* and other neutrality test statistics from low depth next-generation sequencing data. *BMC Bioinformatics* **14**, 289 (2013). doi:10.1186/1471-2105-14-289 Medline

73. X. Xu, Ú. Árnason, The complete mitochondrial DNA sequence of the horse, *Equus caballus*: Extensive heteroplasmy of the control region. *Gene* **148**, 357–362 (1994). doi:10.1016/0378-1119(94)90713-7 Medline

74. P. Danecek, J. K. Bonfield, J. Liddle, J. Marshall, V. Ohan, M. O. Pollard, A. Whitwham, T. Keane, S. A. McCarthy, R. M. Davies, H. Li, Twelve years of SAMtools and BCFtools. *Gigascience* **10**, giab008 (2021). doi:10.1093/gigascience/giab008 Medline

75. M. Costa, B. Elguero, C. Ratti, M. Martinez, P4023 Cloned horses: MtDNA heteroplasmy makes difficult the differentiation protocol. *J. Anim. Sci.* **94**, 90 (2016). doi:10.2527/jas2016.94supplement490x

76. C. Wang, H. Li, Y. Guo, J. Huang, Y. Sun, J. Min, J. Wang, X. Fang, Z. Zhao, S. Wang, Y. Zhang, Q. Liu, Q. Jiang, X. Wang, Y. Guo, C. Yang, Y. Wang, F. Tian, G. Zhuang, Y. Fan, Q. Gao, Y. Li, Z. Ju, J. Li, R. Li, M. Hou, G. Yang, G. Liu, W. Liu, J. Guo, S. Pan, G. Fan, W. Zhang, R. Zhang, J. Yu, X. Zhang, Q. Yin, C. Ji, Y. Jin, G. Yue, M. Liu, J. Xu, S. Liu, J. Jordana, A. Noce, M. Amills, D. D. Wu, S. Li, X. Zhou, J. Zhong, Donkey genomes provide new insights into domestication and selection for coat color. *Nat. Commun.* **11**, 6014 (2020). doi:10.1038/s41467-020-19813-7 Medline

77. L. T. Nguyen, H. A. Schmidt, A. von Haeseler, B. Q. Minh, IQ-TREE: A fast and effective stochastic algorithm for estimating maximum-likelihood phylogenies. *Mol. Biol. Evol.* **32**, 268–274 (2015). doi:10.1093/molbev/msu300 Medline

78. V. Lefort, R. Desper, O. Gascuel, FastME 2.0: A Comprehensive, Accurate, and Fast Distance-Based Phylogeny Inference Program. *Mol. Biol. Evol.* **32**, 2798–2800 (2015). doi:10.1093/molbev/msv150 Medline

79. T. Junier, E. M. Zdobnov, The Newick utilities: High-throughput phylogenetic tree processing in the UNIX shell. *Bioinformatics* **26**, 1669–1670 (2010). doi:10.1093/bioinformatics/btq243 Medline

80. C. C. Chang, C. C. Chow, L. C. A. M. Tellier, S. Vattikuti, S. M. Purcell, J. J. Lee, Second-generation PLINK: Rising to the challenge of larger and richer datasets. *Gigascience* **4**, s13742-015-0047-8 (2015). doi:10.1186/s13742-015-0047-8 Medline

81. A. L. Price, N. J. Patterson, R. M. Plenge, M. E. Weinblatt, N. A. Shadick, D. Reich, Principal components analysis corrects for stratification in genome-wide association studies. *Nat. Genet.* **38**, 904–909 (2006). doi:10.1038/ng1847 Medline

82. S. K. Beeson, J. R. Mickelson, M. E. McCue, Exploration of fine-scale recombination rate variation in the domestic horse. *Genome Res.* **29**, 1744–1752 (2019). doi:10.1101/gr.243311.118 Medline

83. J. M. Sparks, B. E. Crowley, Where did people forage in prehistoric Trinidad? Testing the utility of a multi-isotope approach for tracking the origins of terrestrial prey. *J. Archaeol. Sci. Rep.* **19**, 968–978 (2018). doi:10.1016/j.jasrep.2017.08.002